creative commons

COMMONS DEED

저작자표시-비영리-변경금지 2.0 대한민국

이용자는 아래의 조건을 따르는 경우에 한하여 자유롭게

- 이 저작물을 복제, 배포, 전송, 전시, 공연 및 방송할 수 있습니다.

다음과 같은 조건을 따라야 합니다:

저작자표시. 귀하는 원저작자를 표시하여야 합니다.

비영리. 귀하는 이 저작물을 영리 목적으로 이용할 수 없습니다.

변경금지. 귀하는 이 저작물을 개작, 변형 또는 가공할 수 없습니다.

- 귀하는, 이 저작물의 재이용이나 배포의 경우, 이 저작물에 적용된 이용허락조건을 명확하게 나타내어야 합니다.
- 저작권자로부터 별도의 허가를 받으면 이러한 조건들은 적용되지 않습니다.

저작권법에 따른 이용자의 권리는 위의 내용에 의하여 영향을 받지 않습니다.

이것은 이용허락규약(Legal Code)을 이해하기 쉽게 요약한 것입니다.

Disclaimer

dCollection

의학박사 학위논문

Evaluation and prediction of drug transporter-mediated drug-drug interactions of methotrexate using physiologically based pharmacokinetic modeling

생리학 기반 약물동태 모델링을 이용한
메토트렉세이트의 약물 수송체 매개
약물-약물 상호작용 평가 및 예측

2023년 2월

서울대학교 대학원

의학과 협동과정 임상약리학전공

황 세 정

Ph.D. Dissertation of Medical Science

Evaluation and prediction of drug transporter-mediated drug-drug interactions of methotrexate using physiologically based pharmacokinetic modeling

생리학 기반 약물동태 모델링을 이용한
메토트렉세이트의 약물 수송체 매개
약물-약물 상호작용 평가 및 예측

February 2023

Graduate School of Department of Medicine
Seoul National University
Interdisciplinary Program of Clinical Pharmacology Major

Sejung Hwang

생리학 기반 약물동태 모델링을 이용한 메토트렉세이트의 약물 수송체 매개 약물-약물 상호작용 평가 및 예측

지도 교수 정 재 용

이 논문을 의학박사 학위논문으로 제출함
2022년 10월

서울대학교 대학원
의학과 협동과정 임상약리학전공
황 세 정

황세정의 의학박사 학위논문을 인준함
2023년 1월

위 원 장 _____ (인)

부위원장 _____ (인)

위 원 _____ (인)

위 원 _____ (인)

위 원 _____ (인)

Evaluation and prediction of drug transporter-mediated drug-drug interactions of methotrexate using physiologically based pharmacokinetic modeling

Submitting a Ph.D. Dissertation of Medical Science

October 2022

Graduate School of Department of Medicine
Seoul National University
Interdisciplinary Program of Clinical Pharmacology Major

Sejung Hwang

Supervision by Jae-Yong Chung

Confirming the Ph.D. Dissertation written by Sejung Hwang

January 2023

Chair _____(Seal)

Vice Chair _____(Seal)

Examiner _____(Seal)

Examiner _____(Seal)

Examiner _____(Seal)

ABSTRACT

Evaluation and prediction of drug transporter-mediated drug-drug interactions of methotrexate using physiologically based pharmacokinetic modeling

Sejung Hwang
Interdisciplinary Program of Clinical Pharmacology Major
Graduate School of Department of Medicine
Seoul National University

Introduction: Methotrexate is an antifolate agent widely used in the treatment of various diseases, such as rheumatoid arthritis and cancer. As a substrate of various transporters, methotrexate should be monitored carefully when coadministered with other drugs. This study aimed to quantitatively interpret drug-drug interactions (DDIs) of methotrexate mediated by drug transporters using physiologically based pharmacokinetic (PBPK) modeling. According to this study, a mechanistic evaluation and prediction system about drug transporter-mediated DDIs of methotrexate was developed and applied for

personalized pharmacotherapy of methotrexate.

Methods: A randomized, open-label, 4-treatment, 6-sequence, 4-period crossover study (NCT05575297) was conducted to evaluate the effect of rifampicin and febuxostat on methotrexate pharmacokinetics (PK) in healthy volunteers. Subjects received each treatment according to the assigned sequence, and 4-treatments included the administration of a single dose of methotrexate 2.5 mg alone, coadministration of methotrexate with a single dose of rifampicin 600 mg, with febuxostat 80 mg, or both. Blood samples for PK analysis were collected up to 24 hours post-dose. The PBPK model of methotrexate, rifampicin and febuxostat was developed based on the *in vitro* and *in vivo* data, and the performance of the final PBPK model was validated using the clinical study. The final PBPK model was used to quantitatively interpret the methotrexate DDIs and simulated the high-dose methotrexate with administered with febuxostat in cancer patients.

Results: In the clinical study, when methotrexate was coadministered with rifampicin or febuxostat, the systemic exposure of methotrexate increased by 33% and 17%, respectively, compared to those administered alone. When

methotrexate was coadministered with both rifampicin and febuxostat, the systemic exposure increased by 52% compared to those administered alone. The final PBPK model showed a good prediction performance of the observed clinical data. The impact of drug transporter about DDIs on the methotrexate PK was quantitively evaluated based on the sensitivity analysis and simulation using the PBPK model. The PBPK model showed that the presence of febuxostat resulted in increase of AUC_{0-24h} by 30% in virtual cancer patients.

Conclusion: This study investigated the clinical potential activity of febuxostat with rifampicin for the breast cancer resistance protein (BCRP) inhibition. Furthermore, the PBPK model of methotrexate was well developed in this study and can be used as the mechanistic model to predict and evaluate the drug-transporter mediated DDIs of methotrexate with other drugs and contributed to personalized pharmacotherapy.

Keyword: drug-drug interactions, drug transporter, physiologically based pharmacokinetic (PBPK) modeling, methotrexate, pharmacokinetics, personalized pharmacotherapy

Student Number: 2019-28140

Table of Contents

List of Tables

List of Figures

List of Abbreviations

ABC	ATP-binding cassette
ADAM	Advanced dissolution, absorption, metabolism
AUC	Area under the concentration-time curve
AUC_{0-24h}	AUC from zero to 24 hours after administration
AUC_{inf}	AUC from time zero to infinity
AUC_{last}	AUC from time zero to the last observation
BCRP	Breast cancer resistance protein
BMI	Body mass index
B/P	Blood to plasma partition ratio
CI	Confidence interval
CL_{int}	Intrinsic clearance
CL/F	Total apparent clearance
CL_{PO}	Oral clearance
C_{max}	Maximum plasma concentration
CL_R	Renal clearance
CYP	Cytochrome P450
DDI	Drug-drug interaction
DLM	Diffusion layer model

EDTA	K2-ethylenediaminetetraacetic
f_a	Fraction absorbed
f_e	Fraction excreted unchanged in urine
f_u	Fraction unbound in plasma
$f_{u, Gut}$	Fraction unbound of drug in enterocytes
fu_{inc}	Fraction of unbound drug in the *in vitro* incubation
fu_{mic}	Fraction of unbound drug in the *in vitro* microsomal incubation
GMR	Geometric mean ratio
HLM	Human liver microsomes
IRB	Institutional Review Board
IV	Intravenous
J_{max}	Maximal efflux rate
k_a	First order absorption rate constant
K_i	Inhibition constant
K_m	Michaelis-Menten constant
$K_{m:w}$	Bile salt micelle to water partition coefficient
K_p	Tissue to plasma partition coefficient
Log P	Octanol-water partition coefficient
MRP	Multidrug resistance-associated protein

MATE	Multidrug and toxic compound extrusion
NCA	Non-compartmental analysis
OATP	Organic-anion-transporting polypeptides
PBPK	Physiologically based pharmacokinetics
$P_{eff, man}$	Human jejunum effective permeability
P-gp	P-glycoprotein
PK	Pharmacokinetics
pKa	Acid dissociation constant
Q	Blood flow
$t_{1/2}$	Half-life
T_{max}	Time to reach maximum plasma concentration
V_{sac}	Apparent volume of single adjusting compartment
V_{ss}	Steady state volume of distribution
V_z/F	Apparent volume of distribution

Chapter 1. Introduction

1.1. Study Background

Methotrexate is an antifolate agent widely used in the treatment of autoimmune diseases such as rheumatoid arthritis (RA), psoriasis, and Crohn's disease, and various types of cancer such as acute lymphoblastic leukemia [1, 2]. The pharmacokinetics (PK) of methotrexate has been well researched. Methotrexate has a bioavailability of 64-90% [3]. A total of 60-90% of methotrexate is eliminated by kidney, 10-30% is eliminated vis bile and 1-9% is metabolized to 7-hydroxy methotrexate by aldehyde oxidase after intravenous (IV) dosing [2]. Drug transporters are contributed to the methotrexate PK and methotrexate has been investigated as a substrate of various drug transporters – organic anion transporting polypeptides (OATP1B1 and OATP1B3), organic anion transporters (OAT1 and OAT3), multidrug resistance-related protein (MRP2 and MRP4), and breast cancer resistance protein (BCRP) [4, 5]. As methotrexate is a substrate of various transporters, it should be monitored carefully when coadministered with other drugs such as nonsteroidal anti-inflammatory drugs (NSAIDs). Although methotrexate is not highly bound to albumin (46%) and has a low

hepatic extraction ratio, the drug-drug interactions (DDIs) of methotrexate with other drugs such as NSAIDs, antibacterial agents, and proton pump inhibitors are thought to be clinically significant [6]. The one of the known possible mechanisms for these methotrexate DDIs was the inhibition of OAT1/3, MRP2/4, and BCRP [6].

Although methotrexate DDIs with OAT1/3 inhibitors has been investigated, few clinical studies have evaluated the DDIs between methotrexate and OATP1B1/1B3 or BCRP inhibitors [6, 7]. In this study, a DDIs clinical study was conducted to investigate the methotrexate DDIs with OATP1B1/1B3 inhibitors, and a single dose of rifampin was used as an inhibitor of OATP1B1 and 1B3 [8, 9]. This study was the first clinical DDIs study to evaluate the DDIs between methotrexate and rifampicin.

Febuxostat was used as an inhibitor of BCRP to investigate the methotrexate DDIs in this study. Febuxostat was recently found to strongly inhibit BCRP-mediated transport of urate *in vitro*. In addition, febuxostat increased the exposure of sulfasalazine known as a substrate of BCRP in mice, and rosuvastatin in human [10, 11]. Furthermore, febuxostat and its

acyl glucuronide metabolite showed the potent inhibition activity for OAT3 [12]. The overall disposition of drug transporters associated with absorption, distribution, and elimination of methotrexate and inhibition activity of rifampicin and febuxostat is presented in Figure 1.

The DDIs in clinical settings are difficult to extrapolate from those evaluated based on *in vitro* experiments. Furthermore, a discrepancy exists between the results of *in vitro* experiments and the clinical impact attributed to various factors including physiological factors [13]. Therefore, several approaches to predict and evaluate DDIs using previous *in vitro* and *in vivo* data have been developed [14]. Physiologically based pharmacokinetic (PBPK) model was developed in this study to quantitatively interpret the methotrexate DDIs mediated by drug transporters including OATP1B1/1B3 and BCRP [14]. The PBPK modeling is defined as a mathematical model that simulates drug concentration in tissues and blood considering the rate of the drug's absorption into the body, distribution in tissues, metabolism and excretion (ADME) based on physiological, physicochemical and biochemical characteristics of drug [15, 16]. In addition, PBPK modeling is used to quantitatively describe

and predict the PK of drugs, to evaluate DDIs potential and to support clinical study design, dose selection and labeling during drug development [14, 15].

Furthermore, the developed mechanistic model of methotrexate could be used to predict and simulate the drug transporter-mediated DDIs with other drugs and that in special populations such as cancer patients. The results of non-clinical studies for drug transporter-mediated DDIs are not directly related to the clinical response and are difficult to predict in clinical setting due to the complex interactions of various factors [17]. By conjugating the results of the DDIs clinical study with the model, the PBPK model of this study was used to predict drug transporter-mediated DDIs.

1.2. Purpose of Research

The aim of this study is to develop the mechanistic DDIs model of methotrexate reflecting the features of drug transporters, such as OATP1B1/1B3 and BCRP. Based on the PBPK modeling, the effect of drug transporters on the DDIs of methotrexate was evaluated and predicted. In addition, this study investigated the clinical potential of febuxostat as a BCRP inhibitor.

According to this study, a mechanistic evaluation and prediction system for drug transporter-mediated DDIs of methotrexate was developed and applied for the personalized pharmacotherapy of methotrexate.

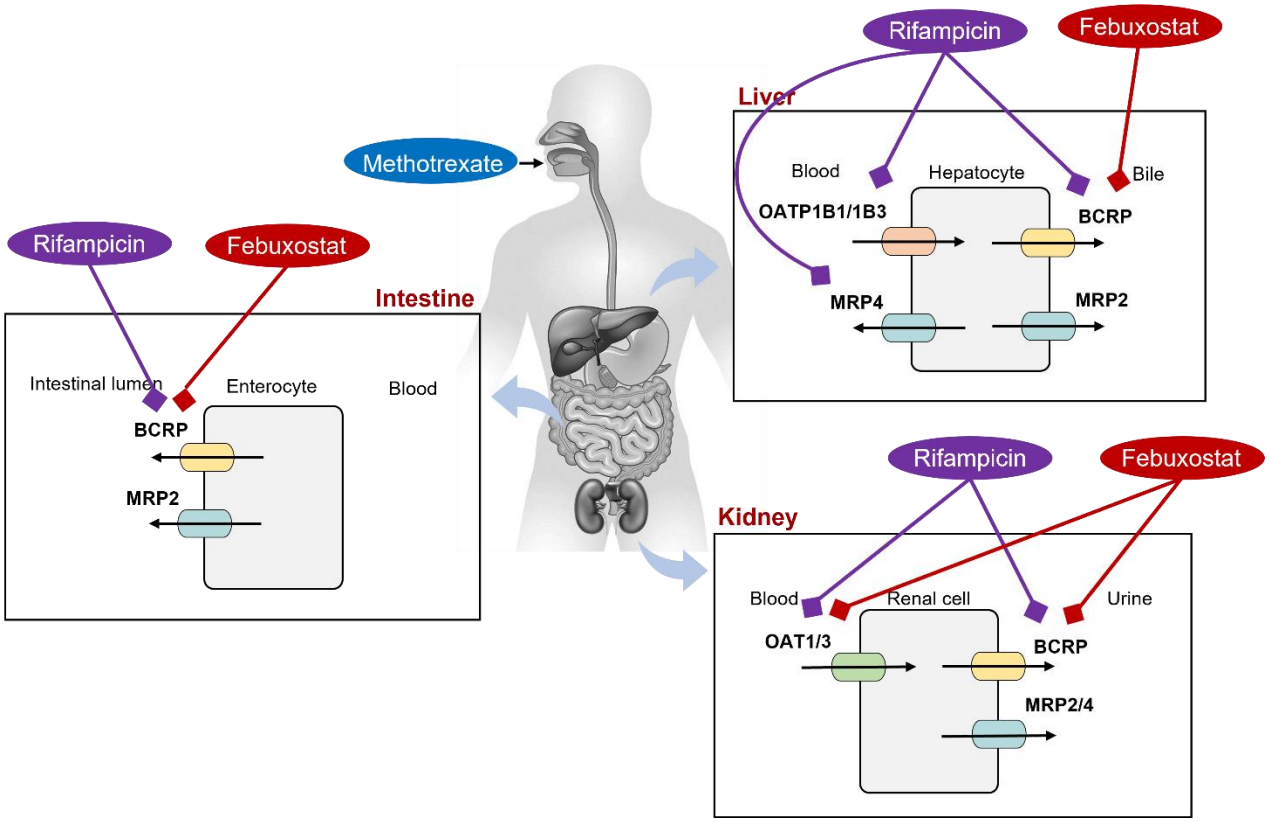

Figure 1. Disposition of drug transporters and inhibition activity of rifampicin and febuxostat associated with the pharmacokinetics of methotrexate.

BCRP, breast cancer resistance protein; MRP, multidrug resistance-associated protein; OAT, organic anion transporter; OATP, organic anion transporting polypeptide

Chapter 2. Methods

Part 1. Clinical Study

2.1.1. Study design and population

The clinical study was approved by the Institutional Review Board (IRB) of Seoul Bundang University Hospital (IRB number: B-2110-715-001, NCT number: NCT05575297). This work was supported by the National Research Foundation of Korea (NRF) grant funded by the Korea government (MSIT) (No. 2021R1F1A1058889). This clinical study was conducted in accordance with the Declaration of Helsinki and Korean Good Clinical Practice (KGCP). Written informed consent was obtained from all subjects before performing any study procedures.

A randomized, open-label, 4-treatment, 6-sequence, 4-period crossover study was conducted. Subjects were randomized in each sequence comprising two subjects, and a total of 12 subjects were planned to complete. In the first period, a single dose of methotrexate 2.5 mg (Methotrexate tab® 2.5 mg, Korean United Pharm. Inc., Korea) was orally administered to all randomized subjects. After the washout period for four days, all subjects received the assigned treatment in the second, third,

and fourth periods according to the sequence. There was a washout period for at least 7 days between the second, third, and fourth periods. One of the following treatments was administered in the second, third, and fourth period according to the assigned sequence: coadministration of a single dose of methotrexate 2.5 mg and a single dose of rifampicin 600 mg (Rifampin tab® 600mg, Yuhan Corporation, Korea), coadministration of a single dose of methotrexate 2.5 mg and a single dose of febuxostat 80 mg (Feburic tab® 80 mg, SK Chemical Co., Ltd., Korea) 12 hours after a single dose of febuxostat 80 mg, and coadministration of methotrexate 2.5 mg, rifampicin 600 mg and febuxostat 80 mg 12 hours after a single dose of febuxostat 80 mg. All subjects received a single dose of folic acid 5 mg 24 hours after the administration of methotrexate to prevent the adverse events (AEs) associated with methotrexate. Blood samples were collected for PK analysis at 0 (before dosing), 0.5, 1, 1.5, 2, 3, 4, 6, 9, 12 and 24 hours after dosing, and urine samples were collected in the time intervals of 0–4, 4–12, 12–24 hours after the methotrexate administration. At each timepoint, the samples were collected using K2–ethylenediaminetetraacetic (EDTA) tubes. The blood samples were centrifuged (approximately 1100 g, 4°C for 10 min), and the separated plasma samples were

stored at −70°C until further analysis. The urine samples were stored at 4 °C after collection, and more than 1 mL sample aliquots were transferred to four Eppendorf tubes for storage at − 70 ℃ until further analysis. The diagram of methotrexate DDIs associated with drug transporters is presented in Figure 2. The overview of clinical study design is presented in Figure 3.

Healthy Korean male subjects aged 19−45 years, and body weight ranging 50.0−90.0 kg with a body mass index (BMI) ranging 18.0−30.0 kg/m^2 were eligible to participate in this study. Subjects who have taken the following drugs or foods were excluded: drugs inducing or inhibiting drug metabolism enzyme/drug transporter such as barbiturates/statin drugs; digoxin within three months before the treatment administration; food containing St. John's Wort and grapefruit within 14 days before the treatment administration; fluid containing caffeine within seven days before the treatment administration. Subjects whose clinical results met the following criteria were excluded: aspartate transaminase, alanine transaminase or total bilirubin was higher than 1.5 times the upper normal limit; white blood cell count was lower than 3,500 /μL; estimated glomerular filtration rate (eGFR) was lower than 60 mL/min/1.73 m^2.

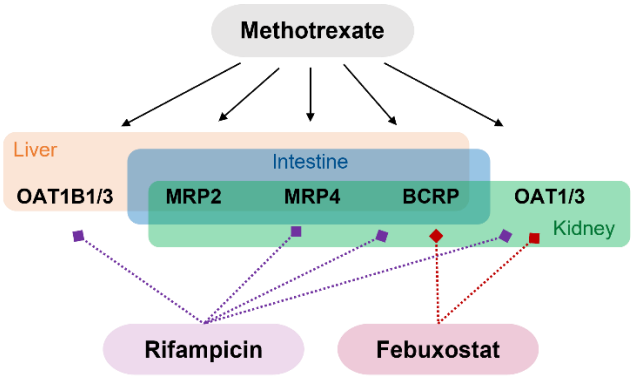

Figure 2. Schematic overview of methotrexate drug-drug interactions associated with drug transporters

OATP, organic anion transporting polypeptide; MRP, multidrug resistance-associated protein; BCRP, breast cancer resistance protein; OAT, organic anion transporter

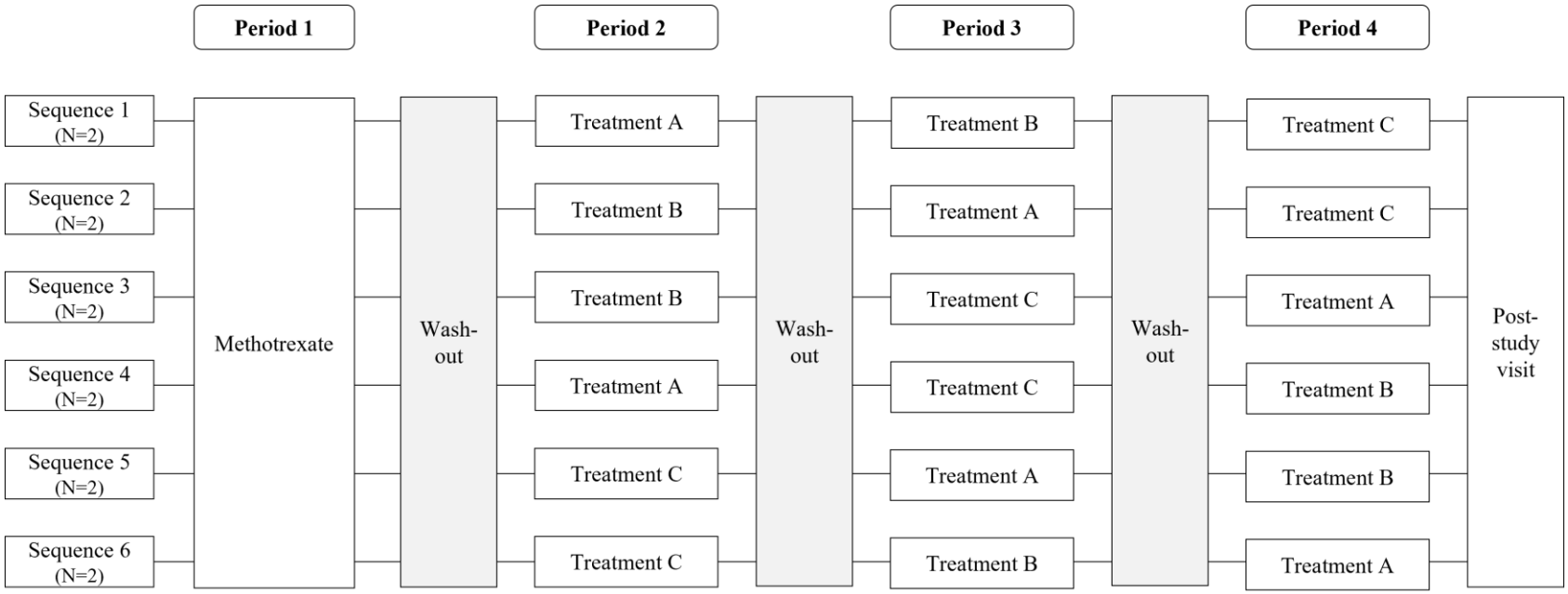

M: Methotrexate
Treatment A: Methotrexate + Rifampicin
Treatment B: Methotrexate + Febuxostat
Treatment C: Methotrexate + Rifampicin + Febuxostat

Figure 3. Clinical study design.

2.1.2. PK evaluation

The plasma concentrations of methotrexate and 7-hydroxy methotrexate and urine concentrations of methotrexate were analyzed by the liquid chromatography–tandem mass spectrometry (LC-MS/MS) system with a valid method.

The PK parameters were estimated by non-compartmental methods using Phoenix WinNonlin software version 8.3 (Pharsight Co, Mountain View, CA). Maximum concentration (C_{max}) and time to reach C_{max} (T_{max}) were obtained from observed concentrations and time. The area under the concentration-time curve (AUC) from zero to the last measurable time point (AUC_{last}) was calculated using the linear up/log down trapezoidal method. The AUC from zero to infinite time (AUC_{inf}) was calculated as $AUC_{last} + C_{last}/\lambda_z$ (C_{last}, the last measurable concentration; λ_z, terminal elimination rate constant). The half-life ($t_{1/2}$) was calculated as $\ln 2/\lambda_z$, and apparent clearance (CL/F) and apparent volume of distribution (V_z/F) was calculated as dose/AUC_{inf} and CL/F/λ_z, respectively. The fraction excreted unchanged in urine (f_e) and renal clearance (CL_R) were also calculated as total amount excreted unchanged/dose and f_e x CL/F.

2.1.3. Statistical Analysis

Statistical analysis was conducted using SAS software version 9.4 (SAS Institute Inc., Cary, NC). Geometric mean ratio (GMR) and 90% confidence intervals (90% CI) were calculated to compare the PK parameters of methotrexate when methotrexate was administered alone and when methotrexate was coadministered with rifampicin, febuxostat, or both.

Part 2. Development of PBPK Model

The workflow for the development and simulation of the PBPK model is presented in Figure 4 and described as follows: PBPK modeling and simulation were conducted using Simcyp simulator Version 21.0 release 1 (Certara, Sheffield, UK). Modelling for the solubility with *in vitro* data was performed using Simcyp In Vitro data Analysis (SIVA) toolkit version 4.0 release 1 (Certara, Sheffield, UK).

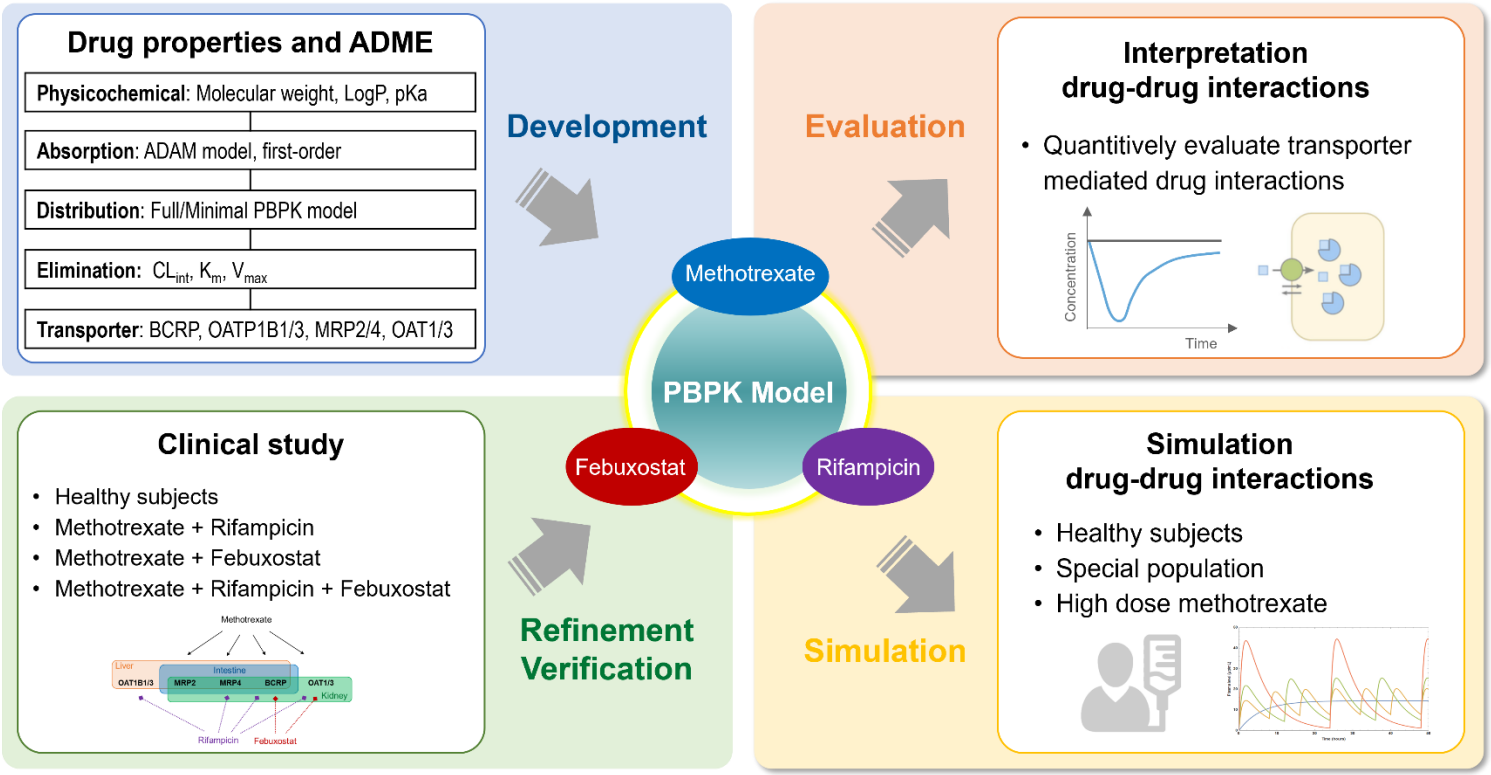

Figure 4. Workflow of physiologically based pharmacokinetic (PBPK) modeling and simulation.

LogP, octanol–water partition coefficient; pK_a, acid dissociation constant; ADAM, advanced dissolution absorption metabolism; CL_{int}, intrinsic clearance; K_m, Michaelis–Menten constant; V_{max}, maximum velocity; BCRP, breast cancer resistance protein; OATP, organic anion transporting polypeptide; MRP, multidrug resistance–associated protein; OAT, organic anion transporter.

2.2.1. PBPK Model of Methotrexate

A full PBPK model for methotrexate was developed based on the literature research including the physiochemical properties and absorption, distribution, metabolism, and excretion properties [18–20]. To develop the absorption model, the Advanced Dissolution, Absorption and Metabolism (ADAM) model was used for the mechanistic absorption modeling along with the diffusion layer model (DLM) [21]. The solubility factor was estimated by SIVA toolkit using the *in vitro* solubility data of methotrexate [22]. The calculated parameters were compared to the experimental solubilities under various pH conditions in SIVA. The bile salt micelle to water partition coefficient for unionized/ionized species ($K_{m:w,unionized/ionized}$) was predicted. The unbound fraction of the drug in enterocytes (f_{ugut}) and the human jejunum effective permeability ($P_{eff,man}$) were predicted using *in vitro* permeability data of methotrexate [23]. The value of MRP2 and BCRP transporter in the transporter was included in the PBPK model because methotrexate is the substrate of MRP2 and BCRP. Methotrexate is also a substrate of other drug transporters – reduced folate carrier (RFC) and proton–coupled folate transporter (PCFT) [24]. Various *in vitro* and *in vivo*

studies have demonstrated that RFC and PCFT is contributed to the intestinal absorption of methotrexate [24-26]. Therefore, the apical uptake of intestine by RFC and PCFT was estimated and reflected in the PBPK model.

For developing the distribution model, a full PBPK model was used, and the steady-state volume of distribution (V_{ss}) was predicted using method 2 suggested by Rodgers and Rowland based on the values of compound characteristics, such as partition coefficient and drug ionization [27, 28].

For the elimination kinetics, a permeability-limited liver model was used to describe the drug transporter-mediated distribution. Transporter kinetics were selected for the application of the elimination to the bile [2]. Previous *in vitro* and *in vivo* studies have investigated that OATP1B1/1B3 contributed to the distribution of methotrexate to the liver [6]. In addition, other *in vitro* studies have shown that methotrexate is the substrate of MRP2/4 and BCRP [29, 30]. Therefore, the values of these transporters were included in the PBPK model of methotrexate [29-31]. Since the primary route of elimination is renal excretion, a mechanistic kidney model (Mech-Kim) was used [2]. Transport across the basolateral membrane of kidney

approximal tubule cells mediated by OAT1/3 is well established, and transport mediated by MRP2/4 located at the apical membrane of kidney proximal tubule cells have been reported to contribute to the renal clearance of methotrexate [32, 33]. The transport mediated by OAT1/3, BCRP, and MRP2/4 in the renal tubule cells was reflected in the PBPK model [29, 34]. Additional intrinsic clearance (CL_{int}) in human liver microsomes (HLM) was included to the model based on the model in the Simcyp library estimated by the clinical data [3]. The final PBPK model input parameters for methotrexate are presented in Table 1.

2.2.2. PBPK model of Rifampicin

The PBPK model for rifampicin was used based on the pre-validated Simcyp compound library. The inhibition of OAT1/3 located in the basolateral membrane and BCRP located in the apical membrane of kidney approximal tubule cells was additionally included [35]. Regarding the inhibition, competitive inhibition of transporter and intrinsic clearance was described by the following Michaelis-Menten equation [36, 37].

$$K_{m,i} = K_m \cdot \left(1 + \frac{I}{K_i}\right) \quad (1)$$

$$CL_{int,inh} = \frac{V_{max}}{K_m \cdot \left(1 + \frac{I_u}{K_{ui}}\right) + S} \quad (2)$$

$K_{m,i}$ is the Michaelis−Menten constant in the presence of inhibitor, I is the concentration of inhibitor, and K_i is the dissociation constant of the inhibitor−transporter complex. $CL_{int,inh}$ is the drug transporter−mediated intrinsic clearance, V_{max} is the maximum velocity of reaction in the absence of an inhibitor, I_u is the unbound concentration at the binding site of drug transporter, K_{ui} is the unbound concentration of inhibitor supporting half maximal inhibition. The K_i value for OAT1/3 and BCRP was calculated from measured inhibitory concentration producing 50% inhibition (IC_{50}) value using the following equation which assumed the Michaelis−Menten kinetics [10, 36].

$$K_i = \frac{IC_{50}}{1 + \frac{S}{K_m}} \quad (3)$$

The final PBPK model input parameters for rifampin are presented in Table 2.

2.2.3. PBPK model of Febuxostat

A minimal PBPK model for febuxostat was constructed based on the literature research [38]. For the absorption, the first-order absorption model was used, and the parameters were included based on the literature [38, 39]. A minimal PBPK model with a single adjusted compartment (SAC) was used to describe the distribution kinetics, and the value of V_{ss} was derived from the previous literature [40]. The values of apparent volume of SAC (V_{sac}) and blood flow between the central compartment and SAC (Q) were included to reflect the biphasic distribution of febuxostat and estimated based on the clinical data (Supplementary Table 2) [41]. The oral *in vivo* clearance (CL_{po}) of febuxostat was used from the results in clinical data (Supplementary Table 2) [39].

The value for the BCRP inhibition was included from the recent *in vitro* and clinical study, which investigated the activity of BCRP inhibition by febuxostat [10, 11]. Competitive inhibition of febuxostat was assumed because the mechanism of action for the BCRP inhibition has not been established. In addition, the inhibition activity of febuxostat for OAT3 has been recently reported [12]. The OAT3 inhibition of febuxostat was also

reflected in the PBPK model of febuxostat in this study [12]. The K_i value of febuxostat was calculated from measured IC_{50} value using equation (3) which assumed the Michaelis−Menten kinetics [10, 36].

In this study, it was assumed that rifampicin and febuxostat inhibit BCRP with the same mechanism. Therefore, the comprehensive effect of p multiple inhibitors with same mechanism was modelled using the following equation [42].

$$CL_{int,inh} = \frac{V_{max}}{K_m \cdot \left(1 + \sum_j^p \frac{I_{u,j}}{K_{ui,j}}\right) + S} \quad (4)$$

$I_{u,j}$ is the unbound concentration of jth inhibitor at the enzyme site and $K_{ui,j}$ is the dissociation constant of jth inhibitor associated with the inhibitor−transporter complex [42]. The final PBPK model input parameters for febuxostat are presented in Table 3.

Table 1. Input parameters for the physiologically based pharmacokinetic model of methotrexate.

Parameter	Value	References/Comments
Physiological chemistry		
Molecular weight (g/mol)	454.44	
Log P	−1.85	
Compound type	Ditropic acid	
pKa1	2.9	Mioduszewska et al., 2017 [19]
pKa2	4.8	Mioduszewska et al., 2017 [19]
B/P	0.68	Herman et al., 1989 [20]
f_u	0.5	Herman et al., 1989 [20]
Absorption		
ADAM model		
f_{uGut}	1	Predicted
$P_{eff,man}$ (x 10^{-4} cm/sec)	0.06	Predicted
MDCK II (x 10^{-6} cm/sec)	0.09	Furubayashi et al., 2020 [23]
Diffusion Layer Model (DLM)		
Intrinsic solubility (mg/mL)	0.01	Fort et al., 1990 [43]
Solubility factor (SF)	5098	Estimated in SIVA [22]
Intrinsic solubility scalar ($S_{o,scalar}$)	32	Yousefi et al., 2010 [22]
$logK_{m:w}$	0.921, −1.079	Predicted
Absorption rate scalar	1	Assumed
Transporter		
Apical uptake		
$CL_{int,T}$ (μL/min/cm^2)	844.28	Estimated

RAF/REF	1	Assumed
MRP2 / apical efflux		
$J_{max, MRP2}$ (pmol/min/10^6 cells)	24	El-Sheikh et al., 2007 [29]
K_m (μM)	480	El-Sheikh et al., 2007 [29]
RAF/REF	2.12	Harwood et al., 2013 [44]
BCRP / apical efflux		
$J_{max,BCRP}$ (pmol/min/10^6 cells)	206.1	Chen et al., 2003 [30]
K_m (μM)	1340	Chen et al., 2003 [30]
RAF/REF	1.19	Harwood et al., 2013 [44]
Distribution		
Full PBPK Model		
V_{ss} (L/kg)	0.39	Predicted using method 2 [28]
K_p scalar	1	Assumed
Elimination		
CL_{int} (HLM) (μL/min/mg protein)	0.24	Simcyp database
Permeability limited liver model		
OATP1B1 / sinusoidal uptake		
$CL_{int,T, OATP1B1}$ (μL/min/10^6 cells)	175.38	Estimated
RAF/REF	1.4	Badee et al., 2015 [45]
OATP1B3 / sinusoidal uptake		
$CL_{int,T, OATP1B3}$ (μL/min/10^6 cells)	150.02	Estimated
RAF/REF	1.11	Badee et al., 2015 [45]
MRP4 / sinusoidal efflux		
$J_{max, MRP4}$ (pmol/min/10^6 cells)	84	El-Sheikh et al., 2007 [29]
K_m (μM)	220	El-Sheikh et al., 2007 [29]
RAF/REF	1	Assumed

MRP2 / canicular efflux		
$J_{max, MRP2}$ (pmol/min/10^6 cells)	24	El−Sheikh et al., 2007 [29]
K_m (μM)	480	El−Sheikh et al., 2007 [29]
RAF/REF	1	Assumed
BCRP / canicular efflux		
$J_{max, BCRP}$ (pmol/min/10^6 cells)	206.1	Chen et al., 2003 [30]
K_m (μM)	1340	Chen et al., 2003 [30]
RAF/REF	1	Assumed
Mechanistic kidney model		
OAT1 / basal uptake		
$CL_{int,T, OAT1}$ (μL/min/10^6 cells)	10	Mathialagan et al., 2017 [46]
RAF/REF	0.64	Mathialagan et al., 2017 [46]
OAT3 / basal uptake		
$J_{max, OAT3}$ (pmol/min/10^6 cells)	80	Kurata et al., 2014 [34]
K_m (μM)	76.6	Kurata et al., 2014 [34]
RAF/REF	4.1	Mathialagan et al., 2017 [46]
MRP2 / apical efflux		
$J_{max, MRP2}$ (pmol/min/10^6 cells)	24	El−Sheikh et al., 2007 [29]
K_m (μM)	480	El−Sheikh et al., 2007 [29]
RAF/REF	1	Assumed
MRP4 / apical efflux		Transporter / function
$J_{max, MRP4}$ (pmol/min/10^6 cells)	84	El−Sheikh et al., 2007 [29]
K_m (μM)	220	El−Sheikh et al., 2007 [29]
RAF/REF	1	Assumed
BCRP / apical efflux		

$J_{max, BCRP}$ (pmol/min/10^6 cells)	206.1	Chen et al., 2003 [30]
K_m (μM)	1340	Chen et al., 2003 [30]
RAF/REF	1	Assumed

Log P, octanol−water partition coefficient; pK_a, acid dissociation constant; B/P, blood to plasma partition ratio; f_u, fraction unbound in plasma; ADAM, advanced dissolution absorption metabolism; f_{uGut}, unbound fraction of drug in enterocytes; $P_{eff,man}$, human jejunum effective permeability; $K_{m:w}$, bile salt micelle to water partition coefficient; J_{max}, maximal efflux rate; K_m, Michaelis−Menten constant; RAF/REF, relative activity/expression factors; MRP, multidrug resistance−associated protein; BCRP, breast cancer resistance protein; V_{ss}, volume of distribution at steady state; K_p, tissue to plasma partition coefficient; $CL_{int,T}$, intrinsic clearance of transporter; OATP, organic anion transporting polypeptide; OAT, organic anion transporter

Table 2. Input parameters for the physiologically based pharmacokinetic model of rifampicin.

Parameter	Value	References/ Comments
Physiological chemistry		
Molecular weight (g/mol)	823	Simcyp Library v21
Log P	4.01	Simcyp Library v21
Compound type	Ampholyte	Simcyp Library v21
pKa1	1.7	Simcyp Library v21
pKa2	7.9	Simcyp Library v21
B/P	0.9	Simcyp Library v21
f_u	0.116	Simcyp Library v21
Absorption		
ADAM Model		
f_{uGut}	1	Simcyp Library v21
$P_{eff,man}$ (x 10^{-4} cm/sec)	2.15	Simcyp Library v21
Caco−2 (x 10−6 cm/sec)	15	Simcyp Library v21
Absorption rate scalars	1	Simcyp Library v21
Distribution		
Full PBPK Model		
V_{ss} (L/kg)	0.42	Simcyp Library v21
K_p scalar	0.0976	Simcyp Library v21
Elimination		
CL_{int} (HLM) (μL/min/mg protein)	2.84	Simcyp Library v21
CL_{int} (Bile) (μL/min/10^6 cells)	0.288	Simcyp Library v21
CL_R (L/h)	1.26	Simcyp Library v21
Inhibition		
CYP		
$K_{i,\ CYP2C8}$ (μM)	24.5	Simcyp Library v21
$K_{i,\ CYP3A4}$ (μM)	24.5	Simcyp Library v21
Transporters (Intestine)		
$K_{i,\ P-gp\ (apical)}$ (μM)	4.3	Simcyp Library v21

$K_{i,\ BCRP\ (apical)}$ (μM)	12.54	Simcyp Library v21
Transporters (Liver)		
$K_{i,\ NTCP\ (sinusoidal)}$ (μM)	187.65	Simcyp Library v21
$K_{i,\ OATP1B1\ (sinusoidal)}$ (μM)	0.162	Simcyp Library v21
$K_{i,\ OATP1B3\ (sinusoidal)}$ (μM)	0.088	Simcyp Library v21
$K_{i,\ OATP2B1\ (sinusoidal)}$ (μM)	0.023	Simcyp Library v21
$K_{i,\ MRP4\ (sinusoidal)}$ (μM)	87.42	Simcyp Library v21
$K_{i,\ P-gp\ (canicular)}$ (μM)	4.3	Simcyp Library v21
$K_{i,\ BCRP\ (canicular)}$ (μM)	12.54	Simcyp Library v21
Transporters (Kidney)		
$K_{i,\ OAT1\ (basal)}$ (μM)	24.05	Estimated using in vitro data (Parvez et al., 2016 [35])
$K_{i,\ OAT3\ (basal)}$ (μM)	15.1	Estimated using in vitro data (Parvez et al., 2016 [35])
$K_{i,\ BCRP\ (apical)}$ (μM)	12.54	Simcyp Library v21

Log P, octanol-water partition coefficient; pKa, acid dissociation constant; B/P, blood/plasma partition ratio; f_u, unbound fraction in plasma; ADAM, advanced dissolution absorption metabolism; fu_{Gut}, unbound fraction of drug in enterocytes; $P_{eff,man}$, human jejunum effective permeability; V_{ss}, volume of distribution at steady state; K_p, tissue to plasma partition coefficient; CL_{int}, in vitro clearance; HLM, human liver microsome; CL_R, renal clearance; CYP, cytochrome P450; K_i, concentration of inhibitor that supports half maximal inhibition; P-gp, p-glycoprotein; BCRP, breast cancer resistance protein; NTCP, sodium (Na+) taurocholate co-transporting polypeptide; OATP, organic anion transporting polypeptide; MRP, multidrug resistance-associated protein; OAT, organic anion transporter

Table 3. Input parameters for the physiologically based pharmacokinetic model of febuxostat.

Parameter	Value	References/Comments
Physiological chemistry		
Molecular weight (g/mol)	316.4	Kamel et al., 2017 [38]
Log P	3.52	Kamel et al., 2017 [38]
Compound type	Monotropic acid	Kamel et al., 2017 [38]
pKa	3.3	Kamel et al., 2017 [38]
B/P	0.645	Xu et al., 2022 [47]
f_u	0.992	Xu et al., 2022 [47]
Absorption		
First order absorption model		
f_a	0.85	Kamel et al., 2017 [38]
k_a (h^{-1})	3.62	Kamel et al., 2022 [39]
fu_{Gut}		
$P_{eff,man}$ (10^{-4} cm/s)	1.64	Xu et al., 2022 [47]
Distribution		
Minimal PBPK model		
Q (L/h)	6.68	Estimated
V_{sac} (L/kg)	0.58	Estimated
V_{ss} (L/kg)	0.7	Khosravan et al., 2006 [40]
Elimination		
CL_{po} (L/h)	7.2	Xu et al., 2022 [47]
Transport inhibition		
Intestine		
$K_{i,\ BCRP\ (apical)}$ (μM)	0.0135	Estimated using *in vitro* data (Miyata et al., 2016 [10])

fu_{inc}	0.022	Miyata et al., 2016 [10]
Liver		
$K_{i,\ BCRP\ (canicular)}$ (μM)	0.0135	Estimated using *in vitro* data (Miyata et al., 2016 [10])
fu_{inc}	0.022	Miyata et al., 2016 [10]
Kidney		
$K_{i,\ BCRP\ (apical)}$ (μM)	0.0135	Estimated using *in vitro* data (Miyata et al., 2016 [10])
fu_{inc}	1	Assumed
$K_{i,\ OAT3\ (basal)}$ (μM)	0.55	Tang et al., 2022 [12]
fu_{inc}	1	Assumed

Log P, octanol−water partition coefficient; pKa, acid dissociation constant; B/P, blood/plasma partition ratio; f_u, fraction unbound in plasma; f_a, fraction available from dosage form; k_a, first order absorption rate constant; Q, blood flow; V_{SAC}, volume of the single adjusted compartment; V_{ss}, volume of distribution at steady state; CL_{po}, oral clearance; K_i, concentration of inhibitor that supports half maximal inhibition; BCRP, breast cancer resistance protein; fu_{inc}, fraction of unbound drug in the *in vitro* incubation

2.2.4. Validation and Evaluation of PBPK Model

The PBPK model of methotrexate, rifampicin and febuxostat was validated using the clinical data conducted in this study and the previous clinical data, respectively (Supplementary Material) [41, 48]. The simulation for validation was conducted for 10 trials of 10 subjects using Sim-Healthy Volunteer population built in the Simcyp simulator. The performance of developed PBPK model was evaluated by comparison of the predicted plasma concentration-time profiles to the observed data in the clinical study. In addition, the ratio of predicted to the observed value ($R_{pred/obs}$) for C_{max}, AUC, and CL_R was calculated and assessed within two-fold range for the evaluation of the performance.

The predicted and observed ratio of C_{max} and AUC were calculated and evaluated using Guest limits following equations to validate the DDIs performance of PBPK model [49]. These limits are used to avoid bias with high prediction accuracy at lower interaction levels.

$$Guest\ limit = \frac{\sigma + 2(R_{obs} - 1)}{R_{obs}} \quad (5)$$

$$Upper\ limit = R_{obs} \times Guest\ limit \quad (6)$$

$$Lower\ limit = R_{obs}/Guest\ limit \quad (7)$$

σ is a parameter that accounts for variability, and the value is 1.25 in this study corresponded to the conventional PK variability of 20%. R_{obs} is the observed ratio of PK parameters when drugs are coadministered to those when victim drug is administered alone.

Global sensitivity analysis was performed to quantitatively evaluate the effect of each transporter on DDIs of methotrexate.

2.2.5. Simulation of PBPK Model in Cancer Patients

The systemic exposure associated with high-dose of methotrexate (higher than 500 mg/m^2) (HDMX) was also investigated in cancer patients using Sim-Cancer population built in the Simcyp simulator. HDMTX higher than 1 g/m^2 is widely used for the treatment of various malignancies, and tumor lysis syndrome (TLS) commonly occurs in hematological malignancy patients [50]. The PK of methotrexate was simulated using Sim-Cancer population when methotrexate 3.5 g/m^2 IV as weekly and

febuxostat 120 mg orally once daily for 10 cycles was coadministered with the dosage regimens based on the reported clinical study [50–52].

Chapter 3. Results

Part 1. Clinical Study

3.1.1. Clinical Study population

A total of 13 healthy Korean male subjects were enrolled, and 11 subjects completed the study. One subject withdrew his consent before the administration of investigational product (IP). One subject withdrew his consent after period two and dropped out after period two. The mean ± standard deviation of age, height, weight, and body mass index (BMI) of 12 enrolled subjects who had received any treatment at least once was 29.5 ± 7.48 years, 173.92 ± 6.41 cm, 68.98 ± 12.20 kg and 22.73 ± 3.20 kg/m^2, respectively. All enrolled subjects were non-smokers.

3.1.2. PK evaluation

The PK analysis was conducted in 12 subjects who received methotrexate alone and received methotrexate with febuxostat and 11 subjects who received methotrexate with rifampicin and received methotrexate with rifampicin and febuxostat. These subjects completed the scheduled procedures for each

treatment.

When methotrexate was administered alone, methotrexate reached the maximum concentration at a median time of 1.0 hour with a range of 0.5 – 2.0 hours (Figure 5, Table 4). When methotrexate was coadministered with rifampicin, methotrexate reached the maximum concentration at a median time of 1.5 hours with a range of 0.5 – 3.0 hours (Figure 5, Table 4). The C_{max}, AUC_{last} and AUC_{inf} of methotrexate increased by 41%, 33%, and 32% respectively compared to those when methotrexate was administered alone (Figure 6, Table 4). The mean half-life and mean CL/F of methotrexate was 2.67 hours and 5.58 L/h, respectively, and slightly decreased compared to those when methotrexate was administered alone (Table 4).

The C_{max} was similar between when methotrexate was administered alone and coadministered with febuxostat (Figure 6, Table 4). The AUC_{last} and AUC_{inf} of methotrexate after co-administration of methotrexate and febuxostat increased by 16 and 17%, respectively, compared to those when methotrexate was administered alone (Figure 6, Table 4). The mean half-life and mean CL/F of methotrexate was 3.10 hours and 6.34 L/h, respectively (Table 4).

When methotrexate was coadministered with both rifampicin and febuxostat, the C_{max}, AUC_{last} and AUC_{inf} of methotrexate increased by 42%, 52%, and 52%, respectively, compared to those when methotrexate was administered alone (Figure 6, Table 4). The mean half-life and mean CL/F of methotrexate was 2.63 hours and 4.85 L/h, respectively, which decreased compared to those when methotrexate was administered alone (Table 4). The mean f_e and CL_R of methotrexate decreased compared to those when methotrexate was administered alone (Table 4).

The PK evaluation of 7-hydroxy methotrexate was described in the Supplementary material.

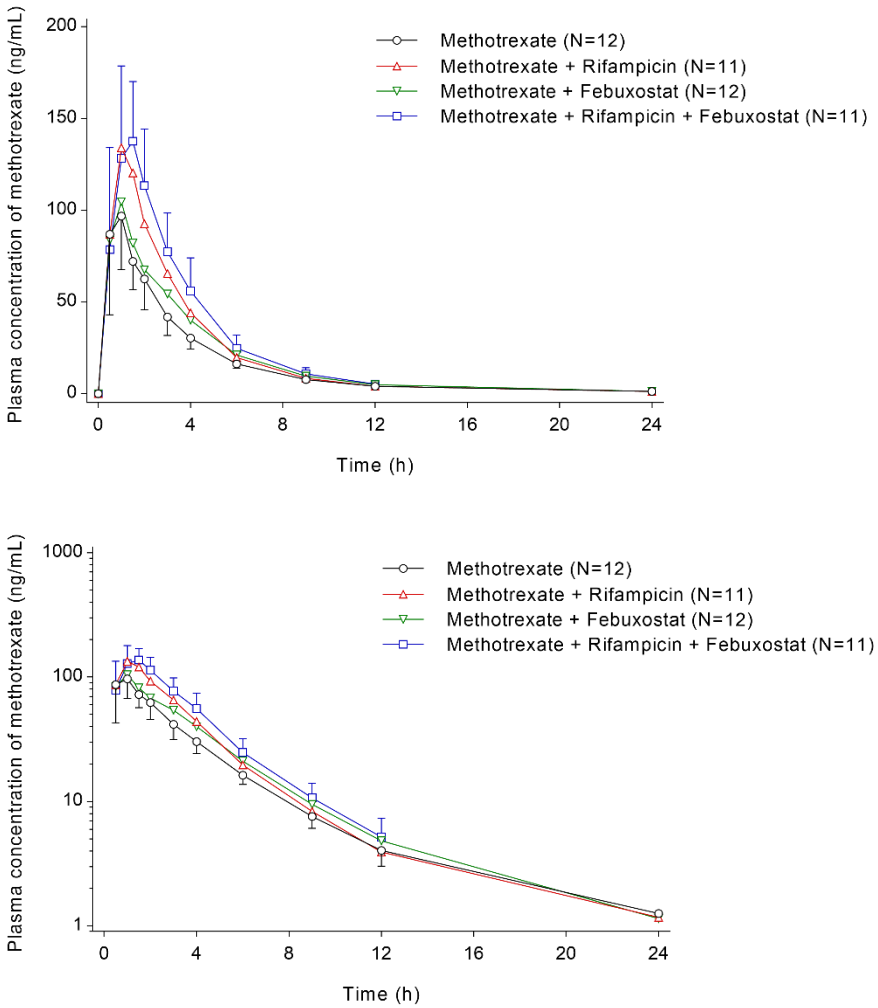

Figure 5. Mean plasma concentration−time profiles of methotrexate after oral administration of methotrexate alone and coadministration with rifampin, febuxostat or both.

Upper panel linear scale, lower panel log scale. The open black circles (◯) and black lines (—) represent the concentrations following oral administration of methotrexate alone. The open red triangles (△) and red lines (—), open green inverted triangles (▽) and green lines (—), and open blue squares (□), and blue lines (—) represent the concentrations following coadministration with rifampicin, febuxostat, or both. The error bars represent standard deviations.

(a)

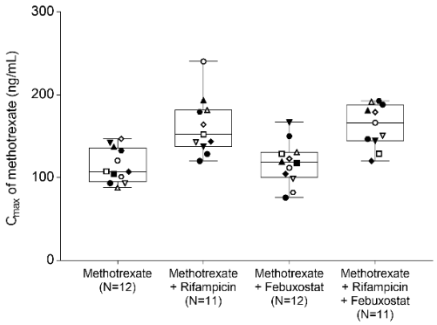

(b)

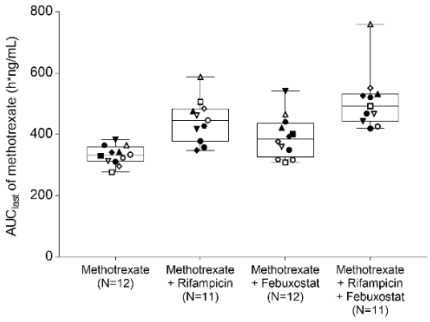

(c)

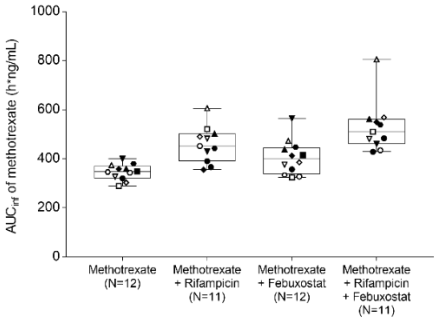

Figure 6. Comparison of (a) C_{max}, (b) AUC_{last} and (c) AUC_{inf} of methotrexate after administration of methotrexate alone and coadministration with rifampin, febuxostat, or both.

The boxes represent the interquartile range (25th to 75th percentile, IQR), horizontal lines represent the median, and the whiskers expand to the minimum and maximum values between the range of 1.5 times of IQR.

Table 4. Pharmacokinetic parameters of methotrexate and geometric mean ratio after the administration of methotrexate alone and coadministration of methotrexate with rifampicin, febuxostat, or both.

	Methotrexate + Rifampicin + Febuxostat (N=11)	GMR (90% CI)[b]	Methotrexate + Febuxostat (N=12)	GMR (90% CI)[c]	Methotrexate + Rifampicin (N=11)	GMR (90% CI)[d]	Methotrexate (N=12)
T_{max} (h)[a]	1.0 (0.5−2.0)	−	1.0 (0.5−3.0)	−	1.5 (0.5−3.0)	−	1.0 (0.5−2.0)
C_{max} (ng/mL)	162.72 ± 25.87	1.42 (1.24−1.61)	117.45 ± 25.93	1.02 (0.90−1.15)	162.20 ± 34.74	1.40 (1.29−1.60)	114.47 ± 20.67
AUC_{last} (h*ng/mL)	509.26 ± 94.13	1.52 (1.44−1.61)	390.72 ± 68.91	1.17 (1.11−1.23)	444.23 ± 70.14	1.33 (1.26−1.41)	331.29 ± 30.49
AUC_{inf} (h*ng/mL)	529.49 ± 103.84	1.52 (1.43−1.61)	404.65 ± 70.42	1.16 (1.10−1.23)	458.2 ± 73.65	1.32 (1.24−1.40)	345.8 ± 32.14
$t_{1/2}$ (h)	2.63 ± 0.28	−	3.10 ± 1.00	−	2.67 ± 0.46	−	3.25 ± 1.07
CL/F (L/h)	4.85 ± 0.77	−	6.34 ± 1.02	−	5.58 ± 0.89	−	7.29 ± 0.70
V_z/F (L)	18.24 ± 2.22	−	28.15 ± 9.09	−	21.35 ± 3.71	−	34.07 ± 11.73
f_e	0.94 ± 0.25	−	0.98 ± 0.16	−	1.10 ± 0.09	−	0.87 ± 0.16
CL_R (L/h)	4.61 ± 1.52	−	6.18 ± 1.34	−	6.13 ± 0.95	−	6.34 ± 1.21

Values are presented as mean ± standard deviation.

[a] Values are presented as median (minimum−maximum).

[b] GMR is calculated as a ratio of geometric mean of methotrexate coadministered with rifampin and febuxostat to that of methotrexate administered alone.

[c] GMR is calculated as a ratio of geometric mean of methotrexate coadministered with febuxostat to that of methotrexate administered alone.

[d] GMR is calculated as a ratio of geometric mean of methotrexate coadministered with rifampicin to that of methotrexate administered alone.

GMR, geometric mean ratio; CI, confidence interval; T_{max}, time to reach to maximum plasma concentration; C_{max}, maximum plasma concentration; AUC_{last}, area under the concentration−time curve (AUC) from zero to last measurable time point; AUC_{inf}, AUC from zero to infinity; $t_{1/2}$, half−life; CL/F, apparent clearance; V_z/F, apparent volume of distribution; f_e, fraction excreted unchanged in urine; CL_R, renal clearance

Part 2. PBPK Modeling

3.2.1. Validation and evaluation of PBPK Model

The developed PBPK model well described the population predicted plasma concentration−time profiles compared to the observed data (Figure 7). The $R_{pred/obs}$ of C_{max} and AUC for methotrexate was within the two−fold range, indicating the good predictive performance of the PBPK model (Figure 9, Table 5). However, the predicted amount excreted unchanged in urine of methotrexate and CL_R was slightly underpredicted compared to the observed data (Figure 8, Table 5). Meanwhile, the predicted ratio of DDIs using PBPK model were within the Guest limits, presenting the good performance of the DDIs prediction (Figure 10).

According to the PBPK model, the clearance and transporter kinetics of methotrexate in liver and kidney were simulated after the coadministration of methotrexate with rifampicin, febuxostat, or both (Figure 11, Figure 12, Supplementary Figure 1). When methotrexate was coadministered with rifampicin or febuxostat, the transport of methotrexate by OAT1B1/1B3 or BCRP was reduced in the liver

(Figure 11, Supplementary Figure 1). The effect of rifampicin on methotrexate CL in liver was extensive. Furthermore, the effect of febuxostat on methotrexate CL in kidney was more extensive than rifampicin (Figure 11, Figure 12). In addition, the additive effect of rifampicin and febuxostat on kidney was also observed (Figure 11, Figure 12).

The impact of drug transporters on the methotrexate PK associated with DDIs was quantitively evaluated based on the sensitivity analysis using the PBPK model (Figure 13). The OATP1B1 and 1B3 had the most influential transporters on the C_{max} and AUC of methotrexate (Figure 13).

3.2.2. Simulation of PBPK model in cancer patients

The verified PBPK models were applied to evaluate the potential risk of DDIs in cancer patients. The plasma and total liver concentration-time profiles of methotrexate were simulated in virtual cancer patients (Figure 14). The C_{max} and AUC_{0-24h} of methotrexate were similar between cycle 1 and cycle 10, representing no accumulation (Figure 15, Table 6). The simulation was conducted in a virtual healthy population with the

same dose regimens of cancer patients to investigate the differences in systemic exposure. When HDMTX was administered alone, simulated AUC_{0-24h} of methotrexate in virtual cancer patients (963.34 h*μg/mL) was higher than that in virtual healthy population (786.25 h*μg/mL) with a 1.23-fold increase. When HDMTX was coadministered with febuxostat, simulated C_{max} ($C_{max,ss}$) and AUC_{0-24h} of methotrexate were also higher than those in the virtual healthy population with a 1.05- and 1.26-fold increase. However, the degree of increase for C_{max} ($C_{max,ss}$) and AUC_{0-24h} after administration of methotrexate alone and coadminitration with febuxostat was similar between virtual cancer patients and healthy population. In virtual cancer patients, the presence of febuxostat resulted in increase of C_{max} ($C_{max,ss}$) and AUC_{0-24h} by 1.09 and 1.30, respectively (Figure 15, Table 6). In the virtual healthy population, the ratio of C_{max} ($C_{max,ss}$) and AUC_{0-24h} when methotrexate was coadministered with febuxostat to those when methotrexate was administered alone were simulated as 1.10 and 1.27, respectively.

(a)

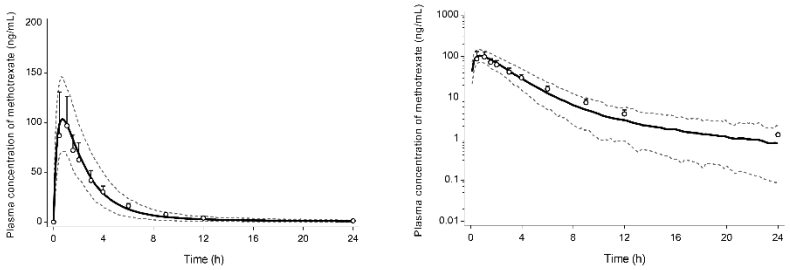

(b)

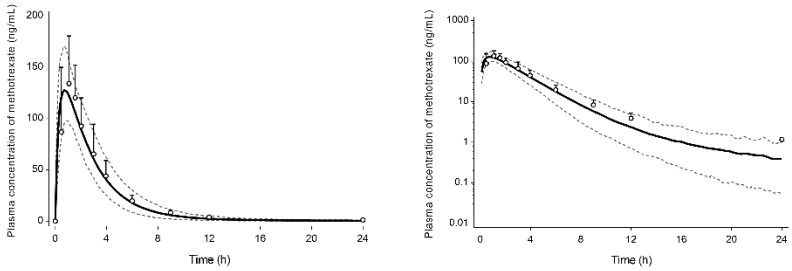

(c)

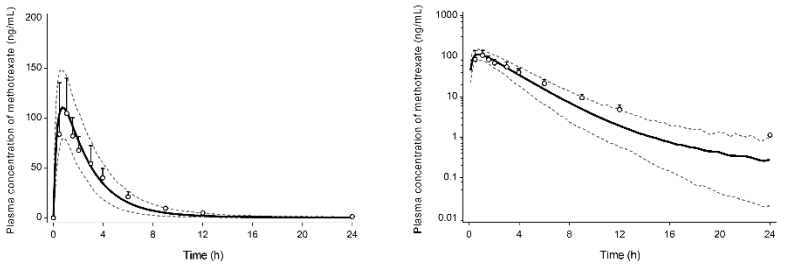

(d)

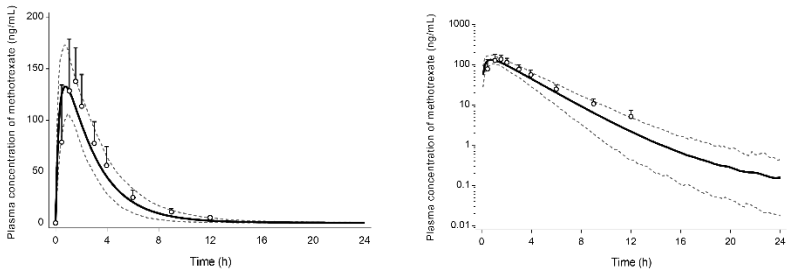

Figure 7. Predicted mean plasma concentration-time profiles of methotrexate after the administration of (a) methotrexate alone and coadministration of methotrexate with (b) rifampicin, (c)

febuxostat or (d) both compared to observed data.

Left panel linear scale, right panel log scale. The solid black line (—) and dashed grey lines (……) represent the predicted mean concentration−time profiles and 5% and 95% percentile of simulation, respectively. The open circles (◯) represent the observed mean concentrations in the clinical study, and the error bars represent standard deviations.

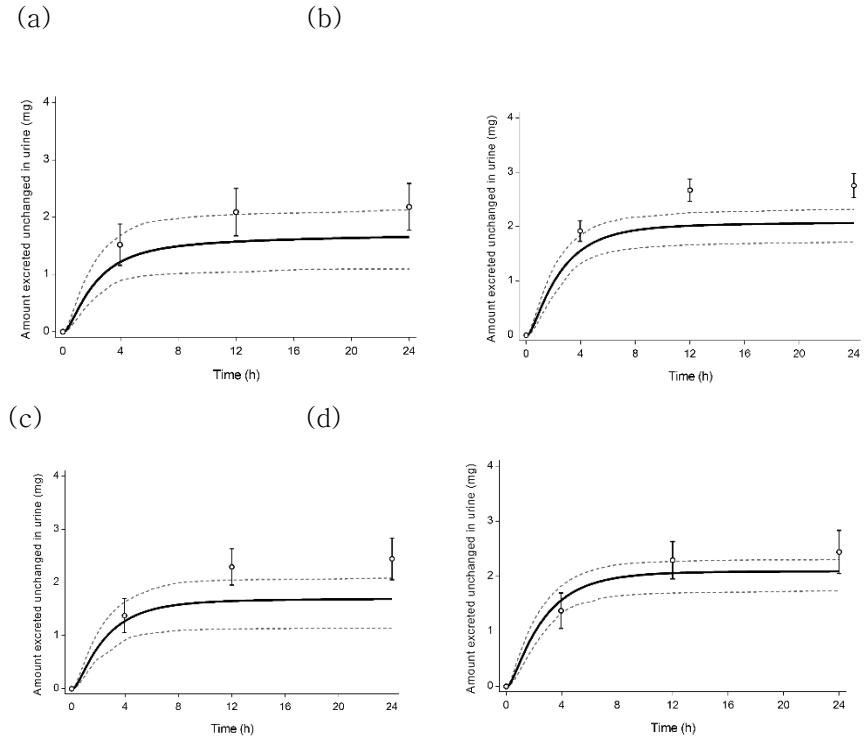

Figure 8. Predicted mean amount excreted unchanged in urine after the administration of (a) methotrexate alone and coadministration of methotrexate with (b) rifampicin, (b) febuxostat, or (c) both compared to observed data.

The solid black line (—) and dashed grey lines (……) represent the predicted mean concentration−time profiles and 5% and 95% percentile of simulation, respectively. The open circles (◯) represent the observed mean concentrations in the clinical study, and the error bars represent standard deviations.

(a)

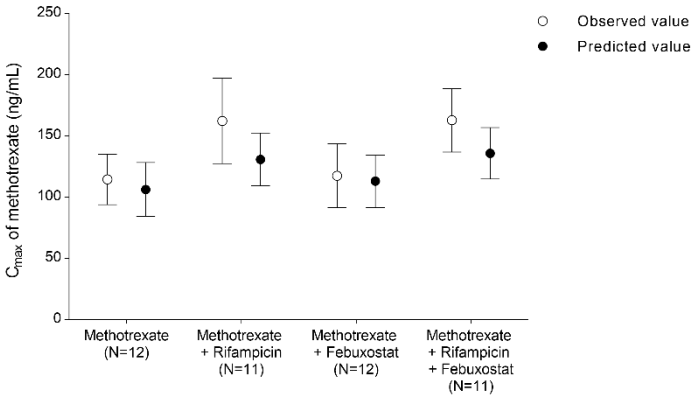

(b)

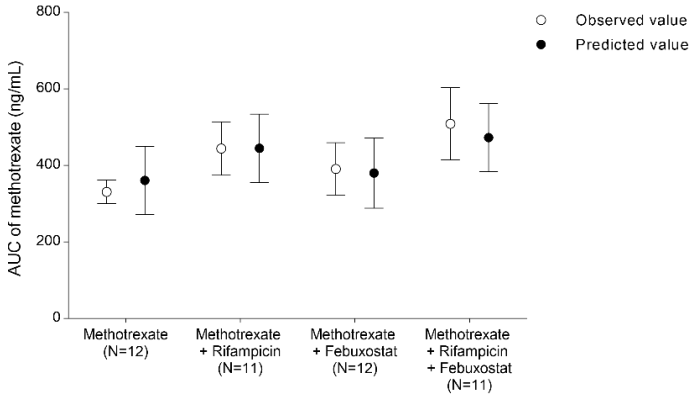

Figure 9. Comparison of mean predicted and observed data for (a) C_{max} and (b) AUC after the administration of methotrexate alone and coadministration of methotrexate with rifampicin, febuxostat, or both.

The black circle (●) and open circle (○) represent mean observed value and mean predicted value, respectively. The error bars represent standard deviations.

C_{max}, maximum concentration; AUC, area under the concentration−time curve

Table 5. Predicted and observed pharmacokinetic parameters of methotrexate after the administration of methotrexate alone and coadministration of methotrexate with rifampicin, febuxostat, or both.

	C_{max} (ng/mL)			AUC_{last} or AUC_{0-24h} (h*ng/mL)			CL_R (L/h)		
	Predicted	Observed	$R_{pred/obs}$	Predicted	Observed	$R_{pred/obs}$	Predicted	Observed	$R_{pred/obs}$
Methotrexate	106.13	114.47	0.93	352.94	331.29	1.07	4.82	6.34	0.76
Methotrexate + Rifampicin	130.66	162.20	0.81	444.76	444.20	1.00	4.79	6.13	0.78
Methotrexate + Febuxostat	112.96	117.45	0.96	380.45	390.72	0.97	4.56	6.18	0.74
Methotrexate + Rifampicin + Febuxostat	135.68	162.72	0.83	473.04	509.26	0.93	4.55	4.61	0.99

C_{max}, maximum plasma concentration; AUC_{last}, area under the concentration−time curve (AUC) from time zero to the last observation; AUC_{0-24h}, AUC from zero to 24 hours after administration; CL_R, renal clearance; $R_{pred/obs}$, the ratio of predicted to the observed value.

(a)

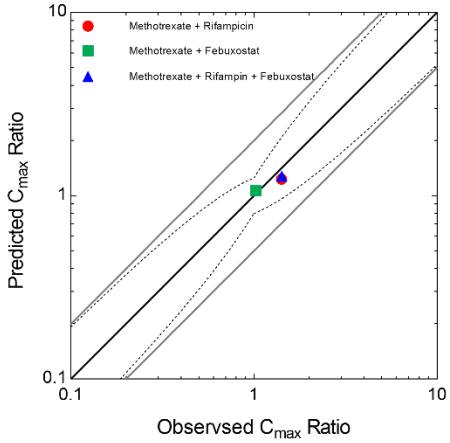

(b)

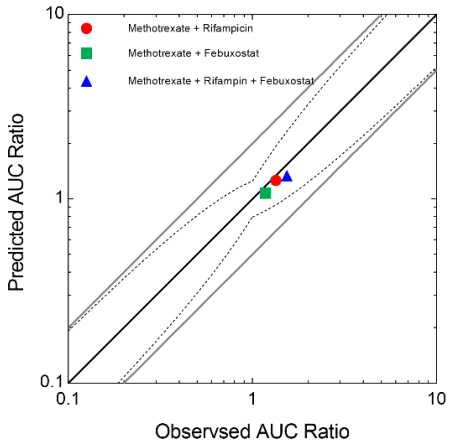

Figure 10. The performance of methotrexate DDI PBPK model. The predicted and observed (a) C_{max} and (b) AUC ratio of methotrexate using Guest limits [49].

DDI, drug-drug interactions; PBPK, physiologically based pharmacokinetic; C_{max}, maximum concentration; AUC, area under the concentration-time curve

(a)

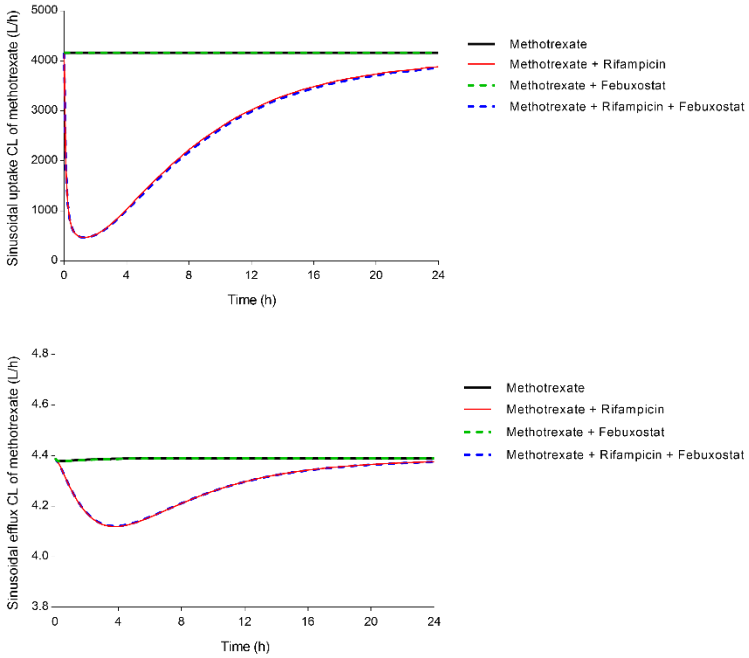

(b)

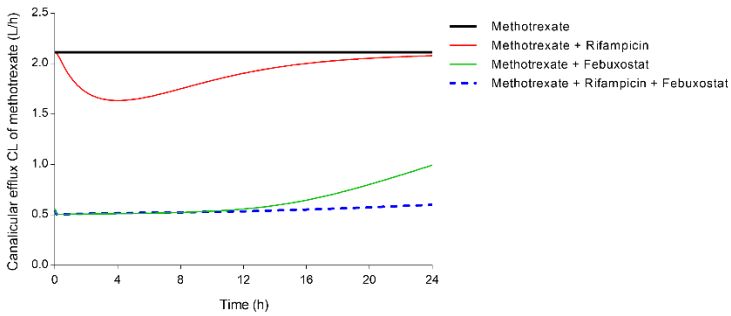

Figure 11. Hepatic clearance of methotrexate by (a) sinusoidal and (b) canicular membrane after administration of methotrexate alone and coadministration of methotrexate with rifampicin, febuxostat, or both.

The black solid line (—), red solid line (—), green solid lines (—) and blue dotted lines (·····) represent the clearance of methotrexate in liver after administration of methotrexate alone and coadministration of rifampicin, respectively.

CL, clearance.

(a)

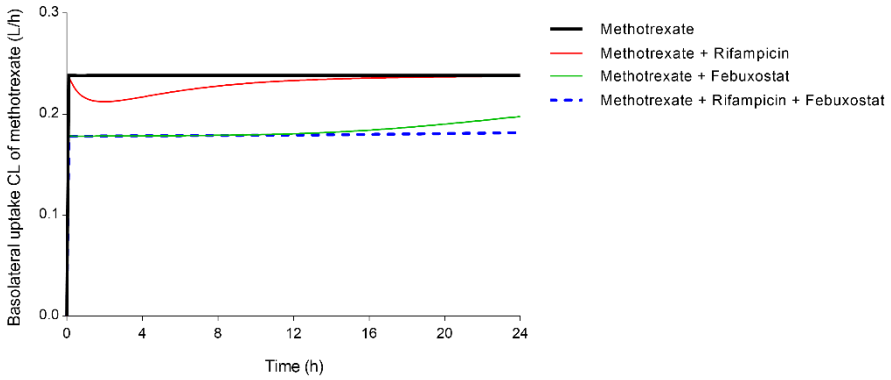

(b)

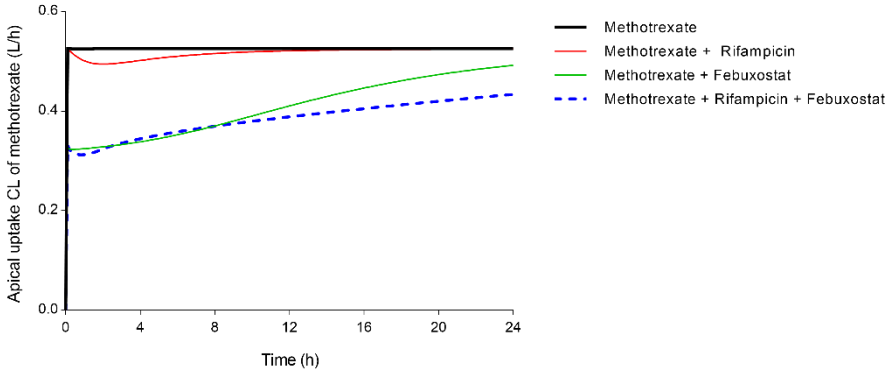

Figure 12. Renal clearance in proximal tubule (segment 1) of methotrexate by (a) basolateral and (b) apical membrane after the administration of methotrexate alone and coadministration of methotrexate with rifampicin, febuxostat or both.

The black solid line (—), red solid line (—), green solid lines (—), and blue botted lines (·····) represent the clearance of methotrexate in kidney proximal tubule after administration of methotrexate alone and coadministration with rifampicin, respectively.

CL, clearance.

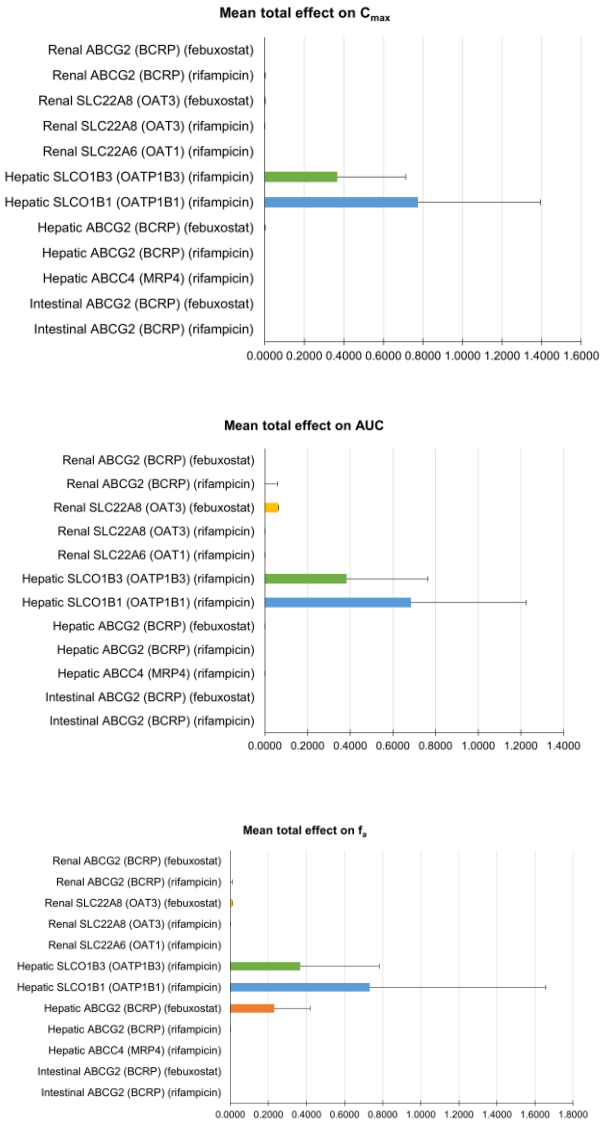

Figure 13. Global sensitivity analysis for methotrexate PK after coadministration of methotrexate with rifampicin and febuxostat.

AUC, area under the concentration–time curve; F_g, the fraction escaping intestinal metabolism; CL_R, renal clearance; BCRP, breast cancer resistance protein; OAT, organic anion transporter; OATP, organic anion transporting polypeptide; MRP, multidrug resistance–associated protein

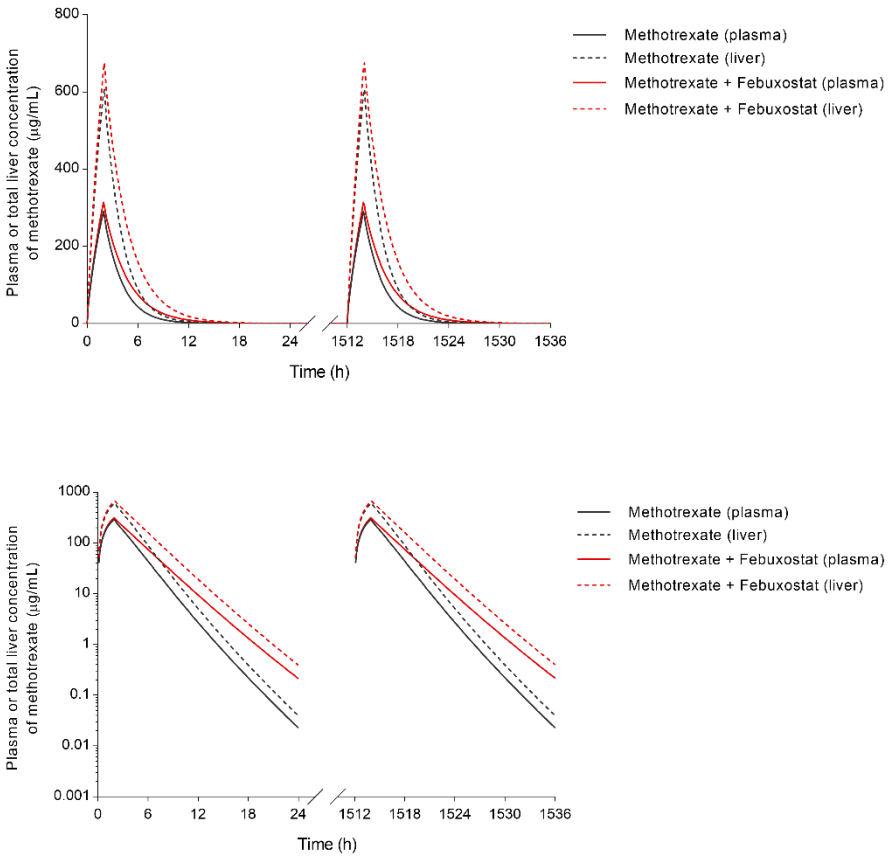

Figure 14. Simulated plasma and total liver concentration-time profiles of methotrexate after the administration of HDMTX alone and the coadministration with febuxostat in cancer patients.

Upper panel linear scale, lower panel log scale. The solid black line (—) and dashed black lines (·····) represent the simulated mean plasma and liver concentration-time profiles, respectively. The solid red lines (—) and dashed red lines (·····) indicate the simulated mean plasma and liver concentration-time profiles when HDMTX was coadministered with febuxostat, respectively.

HDMTX, high-dose methotrexate.

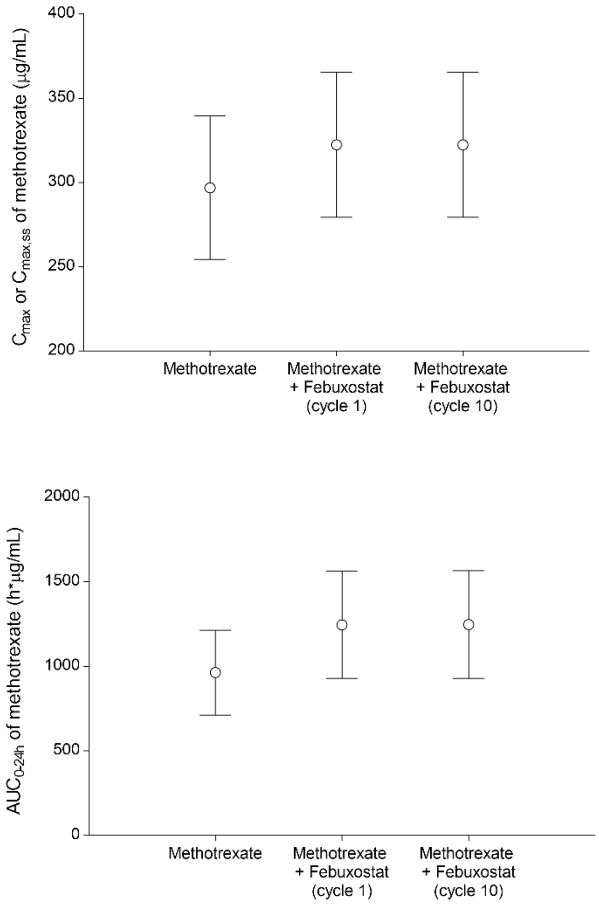

Figure 15. Simulated C_{max} or $C_{max,ss}$ and AUC_{0-24h} of methotrexate after the administration of methotrexate alone and co-administration with febuxostat at cycle 1 and 10.

C_{max}, maximum concentration; $C_{max,ss}$, maximum concentration at steady stat; AUC_{0-24h}, area under the concentration-time curve from zero to 24 hours after administration.

Table 6. Simulated PK parameters of methotrexate in the absence and presence of febuxostat in cancer patients.

Treatment	C_{max} or $C_{max,ss}$ (μg/mL)		AUC_{0-24h} (h*μg/mL)	
	Simulated	Ratio	Simulated	Ratio
Methotrexate 3.5 g/m^2 IV as weekly	296.97	–	963.34	–
Methotrexate 3.5 g/m^2 IV as weekly + Febuxostat 120 mg PO once daily (Cycle 1)	322.41	1.09	1246.33	1.30
Methotrexate 3.5 g/m^2 IV as weekly + Febuxostat 120 mg PO once daily (Cycle 10)	322.44	1.09	1247.50	1.30

Ratio is calculated as a ratio of PK parameters when methotrexate was coadministered with febuxostat to those when methotrexate was administered alone.

C_{max}, maximum concentration; $C_{max,ss}$, maximum concentration at steady-state; AUC_{0-24h}, area under the concentration-time curve from zero to 24 hours after administration; IV, intravenous

Chapter 4. Discussion

The clinical study in this study aimed to investigate the effect of rifampicin and febuxostat on methotrexate PK. A single dose of rifampicin is an inhibitor of various metabolizing enzymes and drug transporters [53]. As previously studies reported, methotrexate is a substrate of various drug transporters [4, 5]. Few clinical studies have evaluated the DDIs of methotrexate and rifampicin despite the potential DDIs associated with drug transporters. In this study, when methotrexate was coadministered with rifampicin, C_{max} and AUC_{last} of methotrexate increased by 40% and 33%, respectively. Considering that methotrexate is a substrate of OATP1B1/1B3, BCRP, MRP4 and OAT1/3, and rifampicin is an inhibitor of these drug transporters, the results of this study were in line with expectations. Because rifampicin and methotrexate were administered orally, the absorption of methotrexate was affected by the BCRP inhibition activity of rifampicin. However, the degree of increase in C_{max} and AUC_{last} of methotrexate in this study was not high compared to that of other substrates of OATP1B1/1B3 and BCRP, rosuvastatin [54]. In that previous study, coadministration of rosuvastatin with rifampicin resulted in an increase of C_{max} and

AUC_{0-24h} by 1025% and 248%, respectively. A comparison of these results showed that the contribution of OATP1B1/1B3 and BCRP to the DDIs of methotrexate and rifampicin was lower than that with rosuvastatin and rifampicin. Rosuvastatin is primarily eliminated in the feces approximately 90%, whereas methotrexate extensively eliminated by kidney almost 90% [2, 55]. In addition, the sinusoidal uptake and efflux and canicular efflux clearance of methotrexate were simulated by the PBPK model, and it was found that the BCRP inhibition by rifampicin was not extensive. Considering the CL_R of methotrexate was similar regardless of the rifampicin coadministration, the OATP1B1/1B3 inhibition of rifampicin in liver was the most influential factors mediating an increase of systemic exposure.

Febuxostat, which has been recently provided as a clinical inhibitor of BCRP by U.S. Food and Drug Administration, increased the systemic exposure of rosuvastatin by 93% when rosuvastatin and febuxostat was coadministered [11, 56]. However, the systemic exposure of methotrexate was increased by 17% in the current study. The concentration of febuxostat in the intestinal lumen may not have been sufficient to inhibit the BCRP in this study. Considering the plasma concentration of

febuxostat and the K_i value of febuxostat required to inhibit the BCRP was 0.0135 μM, it was expected that the concentration of febuxostat was sufficient to inhibit the BCRP. Meanwhile, the $t_{1/2}$ and CL_R of methotrexate were not significantly affected by the coadministration of febuxostat [11].

When methotrexate was coadministered with rifampicin and febuxostat, the C_{max} and AUC_{last} of methotrexate were increased by 42% and 52%, respectively. The BCRP inhibition by febuxostat contributed to the increase in the systemic exposure of methotrexate as the degree of increase was higher compared to that when methotrexate was coadministered with rifampicin. According to the simulation results of canicular efflux clearance in liver by PBPK model, the BCRP inhibition by rifampicin in liver was not extensive when febuxostat was coadministered. In addition, the CL_R of methotrexate extensively decreased when methotrexate was coadministered with rifampicin and febuxostat compared to those with the other interventions. Consequently, the increase in systemic exposure of methotrexate by rifampicin was mediated by the inhibition of OATP1B1/1B3 in liver. Furthermore, the additive effect on the inhibition of drug transporters in kidney mediated by rifampicin and febuxostat

was observed (Figure 16).

Although IV dosing of methotrexate was extensively eliminated by kidney (60−90%), 1−9% of methotrexate was metabolized to 7−hydroxy methotrexate by aldehyde oxidase in liver [2, 57]. The monitoring of 7−hydroxy methotrexate is considered important because it contributes to the safety and methotrexate transport in the cancer patients [58, 59]. In addition, the *in vitro* study suggested that 7−hydroxy methotrexate was transported by BCRP, and the *in vivo* study showed that the systemic exposure increased in MRP2/4 knock−out mouse [60, 61]. In the current clinical study, the PK of 7−hydroxy methotrexate was evaluated to investigate the effect of drug transporter inhibitors. The systemic exposure of 7−hydroxy methotrexate was similar when methotrexate was administered alone and coadministered with febuxostat. In contrast, when methotrexate was coadministered with rifampicin, 7−hydroxy methotrexate was not detected at all time points in 12 subjects. This result suggested that the MRP4 inhibition of sinusoidal efflux by rifampicin was observed in humans, and 7−hydroxy methotrexate is the substrate of MRP4 in human hepatocyte sinusoidal membrane. However, the clinical effect of

the changes in 7-hydroxy methotrexate should be discussed because the dose of methotrexate and the amount of 7-hydroxy methotrexate was low in this clinical study. Febuxostat seemed to be slightly inhibit the biliary excretion of 7-hydroxy methotrexate mediated by BCRP, not extensive degree. To confirm the changes in elimination phase of 7-hydroxy methotrexate, the evaluation of PK profile after 24 hours should be conducted. Therefore, further study about the effect of rifampicin on the systemic exposure and clinical significance of 7-hydroxy methotrexate should be conducted.

In this study, the PBPK model of methotrexate, rifampicin, and febuxostat was developed based on the literature search and the built-in information in the case of rifampicin. The PBPK model of methotrexate has been developed in other studies using Simcyp or MATLAB [2, 62]. However, the PBPK model of methotrexate developed in this study is the first PBPK model reflecting the contribution of drug transporters to the absorption, disposition, and elimination of methotrexate. The PBPK model of methotrexate developed in this study included the intestinal apical uptake describing the transport by RFC and PCFT because the clinical importance of these transporters was emerged and

methotrexate is the substrate of RFC and PCFT [26, 63]. In Simcyp program, since no input parameters are available for MRP2 of the apical efflux in the kidney, the corresponding parameters were inputted as p-glycoprotein (P-gp) instead [64]. In the case of BCRP, the BCRP input parameter were not available for the apical efflux of the kidney in the Simcyp program. Therefore, the input parameters and K_i value for BCRP in the PBPK model was reflected in multidrug and toxic compound extrusion (MATE) parameters because the abundance in virtual population is identical [64]. The PBPK model developed in this study for predicting drug transporters mediated DDI of methotrexate well described the PK profiles and PK parameters except CL_R. The underprediction of CL_R by the PBPK model when methotrexate was administered alone and coadministered with rifampicin or febuxostat might be resulted partly from the measurement errors for the volume of urine and/or methotrexate concentration. Some subjects in this clinical study showed the fraction excreted unchanged in urine greater than 1, and the amount excreted of methotrexate in urine was more than the administered dose (2.5 mg). The PBPK model would not have reflected the amount excreted of methotrexate in urine and

active secretion. Nevertheless, the developed PBPK model well predicted the methotrexate PK, and showed good performance for the DDI prediction by evaluating Guest limits.

Methotrexate is eliminated to the bile (10−30%), and several studies suggested that methotrexate occurred the enterohepatic recirculation (EHC) [2, 5, 65−67]. According to the PBPK model, when methotrexate was coadministered with rifampicin, febuxostat, and both, the amount of bile excretion of methotrexate was decreased by 57%, 73%, and 87%, respectively, compared to that when methotrexate was administered alone. This result suggested that the inhibition of canicular BCRP by rifampicin and febuxostat was successfully reflected in the PBPK model. However, it was simulated that 68% of methotrexate was eliminated to the bile when methotrexate was administered alone. This was a large portion compared to that of previous reported results (8.7−26.0%) [65]. Although the PBPK model simulated the higher portion for the bile excretion, it well described the decrease profiles of bile excretion.

The systemic exposure of methotrexate in virtual cancer patients was simulated using the developed PBPK model in this

study. Tumor lysis syndrome (TLS) is the common treatment-related AEs in patients with hematologic cancers [51]. Febuxostat showed the significant efficacy to control the uric acid levels contributed to the prevention of TLS [51]. The simulation when HDMTX is co-administered with febuxostat was performed based on the dosage regimen reported in the previous clinical studies [50, 51, 68]. One study showed that the concomitant febuxostat could induce hepatotoxicity compared to that without febuxostat [50]. The simulated systemic exposure of methotrexate using the PBPK model increased by 1.30-fold HMTX was coadministered with febuxostat. Additionally, the systemic exposure of HDMTX was also simulated in the virtual healthy population with the same dose regimens in cancer patients. The systemic exposure of methotrexate in the virtual cancer patients was 1.23- to 1.25-fold higher than that in the virtual healthy population. In virtual cancer patients, many physiological factors such as cardiac output and abundance of drug transporters were different from those in the virtual healthy population. For example, the amount of BCRP which contributed to the bile excretion was much lower in the virtual cancer patients, and mechanistic GFR and blood flow in kidney were

lower than that in the virtual healthy population. In liver, the simulated total liver concentrations in the virtual cancer patients were also higher than those in the virtual healthy population. The abundance of BCRP and MRP2 was lower in the virtual cancer population, which contributed to high liver concentrations. According to the results, the increase in systemic exposure of methotrexate by concomitant febuxostat leads to the increase in the incidence of hepatotoxicity. However, the expressions of drug transporters especially ATP-binding cassette (ABC) transporters (P-gp, MRP2/4, BCRP) and the effect of expression on clinical outcomes differ between various cancer types [69, 70]. Therefore, the virtual cancer population built in Simcyp program should be modified if the PBPK model is used for simulation about specific cancer. On the other hand, an increase in the systemic exposure of methotrexate mediated by DDIs could affect the efficacy and dose regimen of methotrexate. As few studies have been discussed the efficacy when the systemic exposure of methotrexate increased by DDIs, the clinical outcome such as dose reduction and prognosis should be further studied.

There are some further considerations of this study.

First, no data corresponding to the genetic polymorphism of drug transporters such as OATP1B1/1B3 are available. Several single nucleotide polymorphisms (SNPs) of solute carrier organic anion transporter *1B1/1B3* (*SLCO1B1/1B3*) encoding OATP1B1/1B3 alter the methotrexate PK and PD [71−73]. The analysis of genetic polymorphism in this study can contribute to the interpretation of the results. Second, the PBPK model was validated by the clinical study data conducted in healthy volunteers. Further studies should be performed to verify the results of the PBPK modeling for the cancer patients and RA patients. Third, in the context of other drug transporters, RFC and PCFT, the PBPK model of methotrexate should be further evaluated and validated. Fourth, because the biliary excretion of methotrexate was higher than previous reported data, the DDIs predicted by the developed PBPK model with drugs influenced in the biliary excretion can be overpredicted. Fifth, as methotrexate is used in various diseases, the doses of methotrexate used in the clinical settings has a wide range more than 100 times with diverse administration routes [52]. The increase in the degree of PK in other doses and clinical impact of the PK changes in the wide range of methotrexate doses should be investigated. Last,

the concentrations of methotrexate glutamates (MTX-PGs) formed in cells by folylpolyglutamate synthetase were not measured and considered in the PBPK modeling. The polyglutamylation of methotrexate leads to intracellular retention and results in altered efficacy along with changes in the activity of autoimmune diseases, such as RA [74-76]. Further research associated with MTX-PGs could be conducted and converged in the results of this study.

Despite these considerations, this study was the first clinical DDIs study to investigate the effect of rifampicin on methotrexate PK. It was also the first study to develop the methotrexate PBPK model that reflected the contributions of drug transporters to the methotrexate PK. In addition, this mechanistic system reflecting the drug transporter-mediated DDIs of methotrexate can be applied to predict the DDIs potential of new drugs and methotrexate.

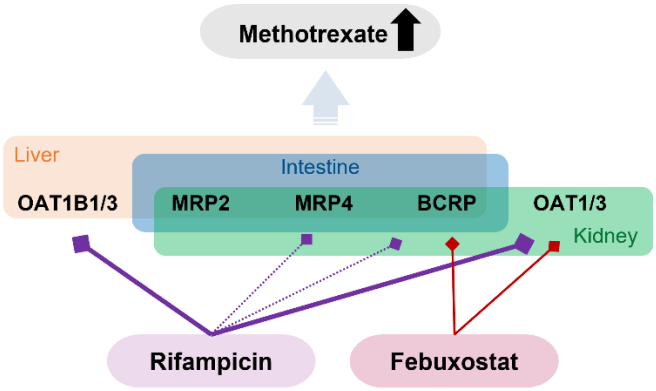

Figure 16. Overview of the effect of rifampicin and febuxostat on methotrexate pharmacokinetics

BCRP, breast cancer resistance protein; OAT, organic anion transporter; OATP, organic anion transporting polypeptide; MRP, multidrug resistance-associated protein

Chapter 5. Conclusion

This study investigated the clinical potential activity of rifampicin and febuxostat for the BCRP inhibition. The OATP1B1/1B3 inhibition by rifampicin in liver resulted in the increase of systemic exposure for methotrexate. The coadministration of methotrexate with rifampicin and febuxostat increased the systemic exposure of methotrexate by the additive inhibition activity of BCRP and OAT3 in the renal tubular cells.

The PBPK model for the prediction of the methotrexate DDIs was well developed and validated in this study. Using the developed the PBPK model, the effect of drug transporters was quantitively evaluated. It was the first study to develop the methotrexate PBPK model reflecting the characteristics of drug transporters. Furthermore, the PBPK model of methotrexate could simulate the methotrexate PK in cancer patients. In conclusion, the DDIs PBPK model developed in this study can be the mechanistic model to predict and evaluate the drug transporter-mediated DDIs of methotrexate with other drugs and contribute to the personalized pharmacotherapy of methotrexate.

Supplementary Material

(a)

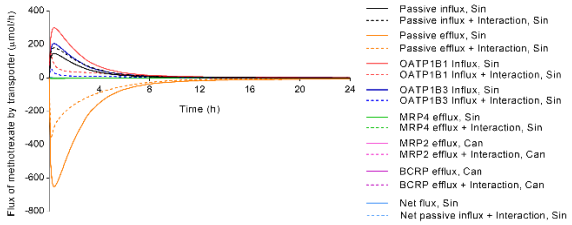

(b)

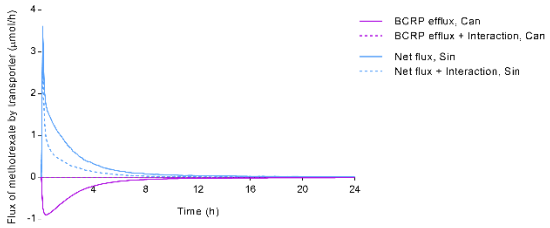

(c)

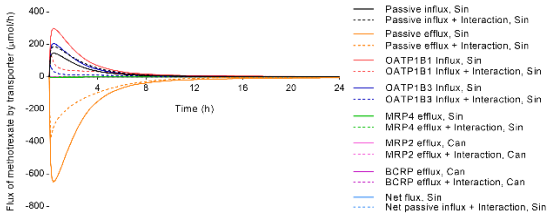

Supplementary Figure 1. Transporter kinetics in liver after coadministration of methotrexate with (a) rifampicin, (b) febuxostat or (c) both.

The solid lines and the dashed lines represent the flux kinetics of methotrexate with interaction and without interaction, respectively. The pink and the sky-blue lines represent OATP1B1 and 1B3 kinetics of methotrexate, respectively. The black and orange lines represent the passive influx and efflux kinetics of methotrexate, respectively. The green and pink lines represent MRP4 and 2 kinetics of methotrexate, respectively. The purple lines represent BCRP efflux kinetics of methotrexate, and the blue lines represent the net flux of sinusoidal side.

Sin, sinusoidal side; Can, canicular; OATP, organic anion transporting polypeptide; MRP, multidrug resistance-associated protein; BCRP, breast cancer resistance protein

1. PK evaluation of 7-hydroxy methotrexate

When methotrexate was administered alone, 7-hydroxy methotrexate reached the maximum concentration at a median time of 6.0 hours with a range of 4.0 – 6.0 hours (Supplementary Figure 2, Supplementary Table 1).

When methotrexate was coadministered with rifampicin, the plasma concentrations of 7-hydroxy methotrexate were not detected at all time points. When methotrexate was coadministered with febuxostat, the C_{max}, AUC_{last} and AUC_{inf} were similar compared to those when methotrexate was administered alone (Supplementary Figure 2, Supplementary Table 1). The metabolic ratio of 7-hydroxy methotrexate was similar with the mean value of 0.14 when methotrexate was administered alone and coadministered with febuxostat (Supplementary Figure 2, Supplementary Table 1). When methotrexate was coadministered with both rifampicin and febuxostat, only 2 subjects showed detectable concentrations of 7-hydroxy methotrexate (Supplementary Table 1). The mean $t_{1/2}$ of 7-hydroxy methotrexate was 15.73 and 12.94 hours when methotrexate was administered alone and coadministered with febuxostat, respectively (Supplementary Table 1).

(a)

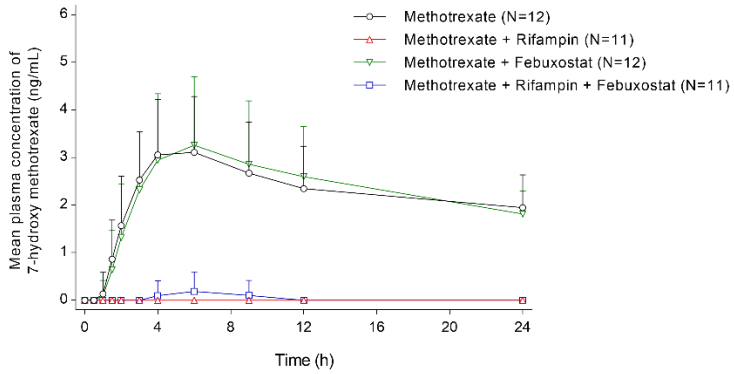

(b)

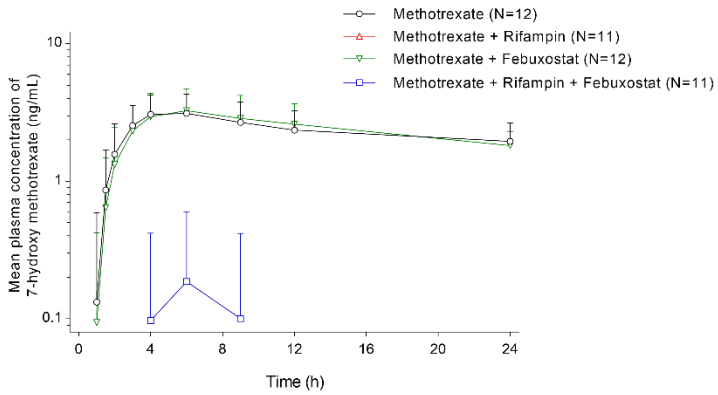

Supplementary Figure 2. Mean plasma concentration−time profiles of 7−hydroxy methotrexate after oral administration of methotrexate alone and coadministration with rifampin, febuxostat, or both. ((a) linear scale, (b) semi−log scale)

The black circles (●) represent the concentrations following oral administration of methotrexate alone, open circles (○) represent the concentrations following coadministration with rifampicin, open triangles (△) represent the concentrations following coadministration with febuxostat, and open inverted triangles (▽) represent the concentrations following coadministration with rifampicin and febuxostat. The error bars represent standard deviations.

Supplementary Table 1. Pharmacokinetic parameters of 7-hydroxy methotrexate and geometric mean ratio after the administration of methotrexate alone and coadministration of methotrexate with rifampicin, febuxostat, or both.

	Methotrexate + Rifampin + Febuxostat (N=11)[b]	GMR (90% CI)[d]	Methotrexate + Febuxostat (N=12)	GMR (90% CI)[f]	Methotrexate + Rifampin (N=11)[g]	Methotrexate (N=12)
T_{max} (h)[a]	.	-	6.0 (4.0-6.0)	-	.	6.0 (4.0-6.0)
C_{max} (ng/mL)	0.19 ± 0.42	0.27 (0.20-0.36)	3.27 ± 1.46	1.00 (0.88-1.12)	.	3.23 ± 1.24
AUC_{last} (h*ng/mL)	3.33 ± 0.97	0.06 (0.03-0.16)	42.4 ± 29.84	0.96 (0.75-1.23)	.	42.1 ± 27.37
AUC_{inf} (h*ng/mL)	.[c]	-	82.09 ± 38.1[e]	0.90 (0.78-1.03)	.	84.73 ± 57.22
$t_{1/2}$ (h)	.	-	12.94 ± 3.4	-	.	15.73 ± 7.39
Metabolic ratio	.	-	0.14 ± 0.1	-	.	0.14 ± 0.09

Values are presented as mean ± standard deviation.

[a] Values are presented as median (minimum-maximum).

[b] N=2; There are 2 subjects who have the concentrations of 7-hydroxy methotrexate.

[c] Terminal elimination constants of two subjects who have the concentrations of 7−hydroxy methotrexate were not estimated.

[d] GMR is calculated as a ratio of geometric mean of 7−hydroxy methotrexate coadministered with rifampin and febuxostat to that of methotrexate administered alone.

[e] N=11; Terminal elimination constant of one subject was not estimated.

[f] GMR is calculated as a ratio of geometric mean of 7−hydroxy methotrexate coadministered with febuxostat to that of methotrexate administered alone.

[g] N=0; No concentrations of 7−hydroxy methotrexate were detected in all subjects.

GMR, geometric mean ratio; CI, confidence interval; T_{max}, time to reach to maximum plasma concentration; C_{max}, maximum plasma concentration; AUC_{last}, area under the concentration−time curve (AUC) from zero to last measurable time point; AUC_{inf}, AUC from zero to infinity; $t_{1/2}$, half−life.

2. Validation of Rifampicin PBPK Model

Methods

The PBPK model of rifampicin in this study was developed based on the built-in model in Simcyp. The previous clinical data was used to validate the inhibition activity of OATP1B1/1B3 in the PBPK model [8, 48]. Because atorvastatin is a substrate of OATP1B1/1B3, the DDI of rifampicin with atorvastatin was evaluated [77]. The clinical data information used for the validation is represented in Supplementary Table 2 [8, 48].

The PBPK model for atorvastatin was developed based on the built-in model in Simcyp. The values of drug transporters that contributed to the absorption of atorvastatin were estimated using the previous clinical data (Supplementary Table 2) [8, 48]. The predicted plasma concentration-time profiles of atorvastatin were compared to the observed data. The simulation for verification was conducted according to the condition of clinical studies. The final PBPK model input parameters for atorvastatin are presented in Supplementary Table 3.

Results

The developed PBPK models of atorvastatin and rifampicin well

predicted the plasma concentration−time profiles of atorvastatin (Supplementary Figure 3).

According to the validation results, the PBPK model of rifampicin developed in this study was the appropriate model reflecting the inhibition activity of OATP1B1/1B3.

Supplementary Table 2. Summary of clinical studies used in PBPK modeling and validation.

No.	Study design	Treatment	Subjects	Analysis	Reference
1	Single dose study	A single 80 mg oral dose of [^{14}C] febuxostat, as a liquid solution	6 (Healthy subjects)	Estimation	Grabowski et al., 2011 [41]
2	Multiple doses, replicate crossover study	Oral daily administration of atorvastatin 40 mg for 7 days	28 (Healthy subjects)	Estimation and validation	Hwang et al., 2021 [48]
3	Randomized, open-label, crossover DDI study	A single oral dose of atorvastatin 40 mg / 30-min IV infusion of rifampin 600 mg + a single oral dose of atorvastatin 40 mg	12 (Healthy subjects)	Estimation and validation	Lau et al., 2007 [8]

Supplementary Table 3. Input parameters for the physiologically based pharmacokinetic model of atorvastatin.

Parameter	Value	References/Comments
Physiological chemistry		
Molecular weight (g/mol)	558.6	Simcyp Library v21
Log P	4.15	Simcyp Library v21
Compound type	Monotropic	Simcyp Library v21
pKa1	4.46	Simcyp Library v21
B/P	0.61	Simcyp Library v21
f_u	0.023	Simcyp Library v21
Absorption		
ADAM Model		
f_{uGut}	1	Simcyp Library v21
$P_{eff,man}$ (x 10^{-4} cm/sec)	2.05	Simcyp Library v21
Caco−2 (x 10^{-6} cm/sec)	8.6	Simcyp Library v21
Absorption rate scalars	1	Simcyp Library v21
Transporter		
P−gp / apical efflux		
$J_{max, P-gp}$ (pmol/min/10^6 cells)	141	El−Sheikh et al., 2007 [29]
K_m (μM)	115	El−Sheikh et al., 2007 [29]
RAF/REF	0.99	Harwood et al., 2013 [44]
Distribution		
Full PBPK Model		
V_{ss} (L/kg)	5.06	Simcyp Library v21
K_p scalar	2.15	Simcyp Library v21
Elimination		
CL_{int} (HLM) (μL/min/mg protein)		Simcyp Library v21
CYP3A4	Pathway 1	

V_{max} (μL/min/pmol)	43.95	Simcyp Library v21
K_m (μM)	28.6	Simcyp Library v21
fu_{mic}	1	Simcyp Library v21
CYP3A4	Pathway 2	
V_{max} (μL/min/pmol)	44.7	Simcyp Library v21
K_m (μM)	24.6	Simcyp Library v21
fu_{mic}	1	Simcyp Library v21
CYP2C8		
V_{max} (μL/min/pmol)	0.12	Simcyp Library v21
K_m (μM)	34.5	Simcyp Library v21
fu_{mic}	1	Simcyp Library v21
UGT1A1		
V_{max} (μL/min/pmol)	2	Simcyp Library v21
K_m (μM)	1.67	Simcyp Library v21
fu_{mic}	1	Simcyp Library v21
UGT1A3		
V_{max} (μL/min/pmol)	38	Simcyp Library v21
K_m (μM)	3.34	Simcyp Library v21
fu_{mic}	1	Simcyp Library v21
UGT2B7		
V_{max} (μL/min/pmol)	3.7	Simcyp Library v21
K_m (μM)	16.72	Simcyp Library v21
fu_{mic}	1	Simcyp Library v21
CL_{int} (Bile) (μL/min/10^6 cells)	0.93	Simcyp Library v21
Permeability limited liver model		
Transporter		Simcyp Library v21
NTCP / sinusoidal uptake		
$J_{max, OATP1B1}$ (pmol/min/10^6 cells)	11759	Estimated (Hwang et al., 2021 [48], Lau et al., 2007 [8])
K_m (μM)	185	Simcyp Library v21

RAF/REF	1	Simcyp Library v21
OATP1B1 / sinusoidal uptake		
$J_{max, OATP1B1}$ (pmol/min/10^6 cells)	294.57	Estimated (Hwang et al., 2021 [48], Lau et al., 2007 [8])
K_m (μM)	0.77	Simcyp Library v21
RAF/REF	1	Simcyp Library v21
OATP1B3 / sinusoidal uptake		
$J_{max, OATP1B3}$ (pmol/min/10^6 cells)	217.7	Estimated (Hwang et al., 2021 [48], Lau et al., 2007 [8])
K_m (μM)	0.73	Simcyp Library v21
RAF/REF	1	Simcyp Library v21
OATP2B1 / sinusoidal uptake		
$J_{max, OATP2B1}$ (pmol/min/10^6 cells)	569.19	Estimated (Hwang et al., 2021 [48], Lau et al., 2007 [8])
K_m (μM)	2.84	Simcyp Library v21
RAF/REF	1	Simcyp Library v21

Log P, octanol−water partition coefficient; pK_a, acid dissociation constant; B/P, blood to plasma partition ratio; f_u, fraction unbound in plasma; ADAM, advanced dissolution absorption metabolism; f_{uGut}, unbound fraction of drug in enterocytes; $P_{eff,man}$, human jejunum effective permeability; P−gp, p−glycoprotein; J_{max}, maximal efflux rate; K_m, Michaelis−Menten constant; RAF/REF, relative activity/expression factors; V_{ss}, volume of distribution at steady state; K_p, tissue to plasma partition coefficient; CL_{int}, intrinsic clearance; CYP, cytochrome P450; V_{max}, maximum rate of metabolism; fu_{mic}, fraction of unbound drug in the in vitro microsomal incubation; UGT, Uridine 5'−diphospho−

glucuronosyltransferase; NTCP, NTCP, sodium (Na+) taurocholate co-transporting polypeptide; OATP, organic anion transporting polypeptide.

(a) (b)

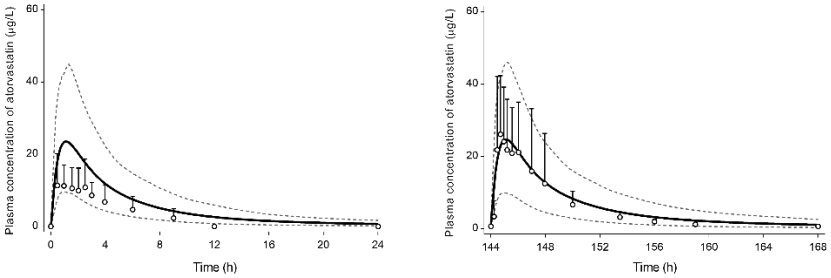

(c)

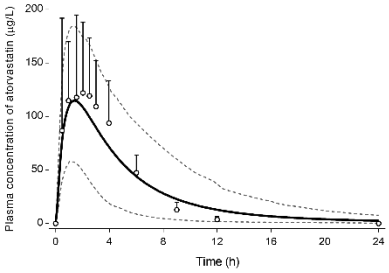

Supplementary Figure 3. Predicted and observed mean plasma concentration–time profiles of atorvastatin after (a) single and (b) multiple administration of atorvastatin alone for 7 days

The solid black line (—) and dashed grey lines (……) represent the predicted mean concentration–time profiles and 5% and 95% percentile of simulation. The open circles (◯) represent the observed mean concentrations in the clinical study, and the error bars represent standard deviations.

Supplementary Table 4. Predicted and observed pharmacokinetic parameters of atorvastatin after the administration of atorvastatin alone and coadministration with rifampicin.

	C_{max} or $C_{max,ss}$ (ng/mL)			AUC_{0-24h} (h*ng/mL)			Reference
	Predicted	Observed	$R_{pred/obs}$	Predicted	Observed	$R_{pred/obs}$	
Atorvastatin (Single dose)	23.87	17.4	1.37	131.66	89.0	1.48	Lau et al., 2007 [8]
Atorvastatin (Multiple doses)	25.04	37.29	0.67	147.40	124.93	1.18	Hwang et al., 2021 [48]
Atorvastatin + Rifampicin	117.14	182.0	1.56	692.46	716.0	1.03	Lau et al., 2007 [8]

C_{max}, maximum plasma concentration; AUC_{0-24h}, area under the concentration−time curve from zero to 24 hours

Bibliography

1. Dominique Levêque, et al., *Clinical pharmacokinetics of methotrexate in oncology.* Int. J. Pharmacokinet, 2017. **2**(2): p. 137-147.
2. Kayode Ogungbenro, Leon Aarons, and T.C.E.-C.P. Groups, *Physiologically based pharmacokinetic modelling of methotrexate and 6-mercaptopurine in adults and children. Part 1: methotrexate.* J Pharmacokinet Pharmacodyn, 2014. **41**(2): p. 159-71.
3. Inoue, K. and H. Yuasa, *Molecular Basis for Pharmacokinetics and Pharmacodynamics of Methotrexate in Rheumatoid Arthritis Therapy.* Drug Metabolism and Pharmacokinetics, 2014. **29**(1): p. 12-19.
4. Erin L. Volk and E. Schneider, *Wild-type breast cancer resistance protein (BCRP/ABCG2) is a methotrexate polyglutamate transporter.* Cancer Res., 2003. **63**(17): p. 5538-5543.
5. Jinzhang Gao, Chun Wang, and W. Wei, *The effects of drug transporters on the efficacy of methotrexate in the treatment of rheumatoid arthritis.* Life Sci, 2021. **268**: p. 118907.
6. Dominique Levêque, et al., *Pharmacokinetic drug-drug interactions with methotrexate in oncology.* Expert Rev Clin Pharmacol., 2011.
7. Selvi Durmus, et al., *Preclinical Mouse Models To Study Human OATP1B1- and OATP1B3-Mediated Drug-Drug Interactions in Vivo.* Mol Pharm, 2015. **12**(12): p. 4259-69.
8. YY Lau, et al., *Effect of OATP1B transporter inhibition on the pharmacokinetics of atorvastatin in healthy volunteers.* Clin Pharmacol Ther, 2007. **81**(2): p. 194-204.
9. Alexander Treiber, et al., *Bosentan is a substrate of human OATP1B1 and OATP1B3: inhibition of hepatic uptake as the common mechanism of its interactions with cyclosporin A, rifampicin, and sildenafil.* Drug Metab Dispos, 2007. **35**(8): p. 1400-7.
10. Miyata, H., et al., *Identification of Febuxostat as a New Strong ABCG2 Inhibitor: Potential Applications and Risks in Clinical Situations.* Front Pharmacol, 2016. **7**: p. 518.
11. Lehtisalo, M., et al., *Febuxostat, But Not Allopurinol, Markedly Raises the Plasma Concentrations of the Breast*

Cancer Resistance Protein Substrate Rosuvastatin. Clin Transl Sci, 2020. **13**(6): p. 1236-1243.
12. Tang, L.W.T., T.W.H. Cheong, and E.C.Y. Chan, *Febuxostat and its major acyl glucuronide metabolite are potent inhibitors of organic anion transporter 3: Implications for drug-drug interactions with rivaroxaban.* Biopharm Drug Dispos, 2022. **43**(2): p. 57-65.
13. Yang, X., et al., *Current Perspective on Residual Knowledge Gaps in the Assessment of Transporter-Mediated Drug Interactions.* Clin Pharmacol Ther, 2022. **112**(3): p. 450-452.
14. Min, J.S. and S.K. Bae, *Prediction of drug-drug interaction potential using physiologically based pharmacokinetic modeling.* Arch Pharm Res, 2017. **40**(12): p. 1356-1379.
15. *European Medicines Agency. Guideline on the reporting of physiologically based pharmacokinetic (PBPK) modeling and simulation. 2018 [cited 2022 May 31]; Avilable from: https://www.ema.europa.eu/en/documents/scientific-guideline/guideline-reporting-physiologically-based-pharmacokinetic-pbpk-modelling-simulation_en.pdf.*
16. Kuepfer, L., et al., *Applied Concepts in PBPK Modeling: How to Build a PBPK/PD Model.* CPT Pharmacometrics Syst Pharmacol, 2016. **5**(10): p. 516-531.
17. Kremers, P., *In vitro tests for predicting crug-drug Interactions: The need for validated procedures.* Pharmacol Toxicol., 2002. **91**(5): p. 209-17.
18. C. Hansch, A. Leo, and D. Hoekman, *Exploring QSAR - hydrophobic, electronic, and steric constants.* . 1995, Washington, DC.: American Chemical Society.
19. Mioduszewska, K., et al., *Overview of experimental and computational methods for the determination of the pKa values of 5-fluorouracil, cyclophosphamide, ifosfamide, imatinib and methotrexate.* TrAC Trends in Analytical Chemistry, 2017. **97**: p. 283-296.
20. Herman, R.A., et al., *Pharmacokinetics of low-dose methotrexate in rheumatoid arthritis patients.* J Pharm Sci, 1989. **78**(2): p. 165-71.
21. Pathak, S.M., et al., *Model-Based Analysis of Biopharmaceutic Experiments To Improve Mechanistic Oral Absorption Modeling: An Integrated in Vitro in Vivo Extrapolation Perspective Using Ketoconazole as a Model Drug.* Mol Pharm, 2017. **14**(12): p. 4305-4320.

22. Gholamhossein Yousefi, et al., *Synthesis and characterization of methotrexate polyethylene glycol esters as a drug delivery system.* Chem Pharm Bull (Tokyo). 2010. **58**(2): p. 147-53.
23. Furubayashi, T., et al., *Comparison of Various Cell Lines and Three-Dimensional Mucociliary Tissue Model Systems to Estimate Drug Permeability Using an In Vitro Transport Study to Predict Nasal Drug Absorption in Rats.* Pharmaceutics, 2020. **12**(1).
24. Visentin, M., et al., *The intestinal absorption of folates.* Annu Rev Physiol, 2014. **76**: p. 251-74.
25. Murakami, T. and N. Mori, *Involvement of Multiple Transporters-mediated Transports in Mizoribine and Methotrexate Pharmacokinetics.* Pharmaceuticals (Basel), 2012. **5**(8): p. 802-36.
26. Shin, D.S., et al., *Functional roles of aspartate residues of the proton-coupled folate transporter (PCFT-SLC46A1); a D156Y mutation causing hereditary folate malabsorption.* Blood, 2010. **116**(24): p. 5162-9.
27. Rodgers, T. and M. Rowland, *Physiologically based pharmacokinetic modelling 2: predicting the tissue distribution of acids, very weak bases, neutrals and zwitterions.* J Pharm Sci, 2006. **95**(6): p. 1238-57.
28. Rodgers, T. and M. Rowland, *Mechanistic approaches to volume of distribution predictions: understanding the processes.* Pharm Res, 2007. **24**(5): p. 918-33.
29. El-Sheikh, A.A., et al., *Interaction of nonsteroidal anti-inflammatory drugs with multidrug resistance protein (MRP) 2/ABCC2- and MRP4/ABCC4-mediated methotrexate transport.* J Pharmacol Exp Ther, 2007. **320**(1): p. 229-35.
30. Zhe-Sheng Chen, et al., *Transport of methotrexate, methotrexate polyglutamates, and 17beta-estradiol 17-(beta-D-glucuronide) by ABCG2: Effects of acquired mutations at R482 on methotrexate transport.* Cancer Res., 2003. **63**(14): p. 4048-54.
31. Patik, I., et al., *Identification of novel cell-impermeant fluorescent substrates for testing the function and drug interaction of Organic Anion-Transporting Polypeptides, OATP1B1/1B3 and 2B1.* Sci Rep, 2018. **8**(1): p. 2630.
32. Takeda, M., et al., *Characterization of methotrexate transport and its drug interactions with human organic*

anion transporters. J Pharmacol Exp Ther, 2002. **302**(2): p. 666-71.
33. Zhe-Sheng Chen, et al., *Analysis of methotrexate and folate transport by multidrug resistance protein 4 (ABCC4): MRP4 is a component of the methotrexate efflux system.* Cancer Res., 2002. **62**(11): p. 2144-50.
34. Kurata, T., et al., *Characteristics of pemetrexed transport by renal basolateral organic anion transporter hOAT3.* Drug Metab Pharmacokinet, 2014. **29**(2): p. 148-53.
35. Parvez, M.M., et al., *Inhibitory Interaction Potential of 22 Antituberculosis Drugs on Organic Anion and Cation Transporters of the SLC22A Family.* Antimicrob Agents Chemother, 2016. **60**(11): p. 6558-6567.
36. Haupt, L.J., et al., *The Reliability of Estimating Ki Values for Direct, Reversible Inhibition of Cytochrome P450 Enzymes from Corresponding IC50 Values: A Retrospective Analysis of 343 Experiments.* Drug Metab Dispos, 2015. **43**(11): p. 1744-50.
37. Cheng, Y.-C. and W.H. Prusoff, *Relationship between the inhibition constant (KI) and the concentration of inhibitor which causes 50 per cent inhibition (I50) of an enzymatic reaction.* Biochem Pharmacol, 1973. **22**(23): p. 3099-108.
38. Kamel, B., et al., *Clinical Pharmacokinetics and Pharmacodynamics of Febuxostat.* Clin Pharmacokinet, 2017. **56**(5): p. 459-475.
39. Kamel, B., et al., *Population pharmacokinetic modelling of febuxostat in healthy subjects and people with gout.* Br J Clin Pharmacol, 2022.
40. Khosravan, R., et al., *The effect of mild and moderate hepatic impairment on pharmacokinetics, pharmacodynamics, and safety of febuxostat, a novel nonpurine selective inhibitor of xanthine oxidase.* J Clin Pharmacol, 2006. **46**(1): p. 88-102.
41. Grabowski, B.A., et al., *Metabolism and excretion of [14C] febuxostat, a novel nonpurine selective inhibitor of xanthine oxidase, in healthy male subjects.* J Clin Pharmacol, 2011. **51**(2): p. 189-201.
42. Rostami-Hodjegan, A. and G. Tucker, *'In silico' simulations to assess the 'in vivo' consequences of 'in vitro' metabolic drug-drug interactions.* Drug Discov Today Technol, 2004. **1**(4): p. 441-8.
43. James J. Fort and A.K. Mitra, *Solubility and stability*

characteristics of a series of methotrexate diakyl esters.pdf. International journal of pharmaceutics, 1990. **59**: p. 271-79.
44. Harwood, M.D., et al., *Absolute abundance and function of intestinal drug transporters: a prerequisite for fully mechanistic in vitro-in vivo extrapolation of oral drug absorption.* Biopharm Drug Dispos, 2013. **34**(1): p. 2-28.
45. Badee, J., et al., *Meta-analysis of expression of hepatic organic anion-transporting polypeptide (OATP) transporters in cellular systems relative to human liver tissue.* Drug Metab Dispos, 2015. **43**(4): p. 424-32.
46. Mathialagan, S., et al., *Quantitative Prediction of Human Renal Clearance and Drug-Drug Interactions of Organic Anion Transporter Substrates Using In Vitro Transport Data: A Relative Activity Factor Approach.* Drug Metab Dispos, 2017. **45**(4): p. 409-417.
47. Yichao Xu, et al., *Simulation of febuxostat pharmacokinetics in healthy subjects and patients with impaired kidney function using physiologically based pharmacokinetic modeling.* Biopharm Drug Dispos, 2022.
48. Hwang, S., et al., *Co-Administration of Vonoprazan, Not Tegoprazan, Affects the Pharmacokinetics of Atorvastatin in Healthy Male Subjects.* Front Pharmacol, 2021. **12**: p. 754849.
49. Guest, E.J., et al., *Critique of the two-fold measure of prediction success for ratios: application for the assessment of drug-drug interactions.* Drug Metab Dispos, 2011. **39**(2): p. 170-3.
50. Ikemura, K., et al., *Concomitant febuxostat enhances methotrexate-induced hepatotoxicity by inhibiting breast cancer resistance protein.* Sci Rep, 2019. **9**(1): p. 20359.
51. Spina, M., et al., *FLORENCE: a randomized, double-blind, phase III pivotal study of febuxostat versus allopurinol for the prevention of tumor lysis syndrome (TLS) in patients with hematologic malignancies at intermediate to high TLS risk.* Ann Oncol, 2015. **26**(10): p. 2155-61.
52. Howard, S.C., et al., *Preventing and Managing Toxicities of High-Dose Methotrexate.* Oncologist, 2016. **21**(12): p. 1471-1482.
53. Mikko Niemi, et al., *Pharmacokinetic interactions with rifampicin: clinical relevance.* Clin Pharmacokinet, 2003. **42**(9): p. 819-50.

54. Wiebe, S.T., et al., *Validation of a Drug Transporter Probe Cocktail Using the Prototypical Inhibitors Rifampin, Probenecid, Verapamil, and Cimetidine.* Clin Pharmacokinet, 2020. **59**(12): p. 1627-1639.
55. Paul D Martin, et al., *Metabolism, excretion, and pharmacokinetics of rosuvastatin in healthy adult male volunteers.* Clin Ther, 2003. **25**(11): p. 2822-35.
56. *U.S. Food and Drug Administration (2022) - Drug development and Drug Interactions | Table of Substrates, Inhibitors and Inducers. Accessed: Nov 17 2022. https://www.fda.gov/drugs/drug-interactions-labeling/drug-development-and-drug-interactions-table-substrates-inhibitors-and-inducers.*
57. Maksimovic, V., et al., *Molecular mechanism of action and pharmacokinetic properties of methotrexate.* Mol Biol Rep, 2020. **47**(6): p. 4699-4708.
58. Lankelma, J., E.v.d. Klein, and F. Ramaekers, *The role of 7-hydroxymethotrexate during methotrexate anti-cancer therapy.* Cancer Lett., 1980. **9**(2): p. 133-42.
59. Joerger, M., et al., *Determinants of the elimination of methotrexate and 7-hydroxy-methotrexate following high-dose infusional therapy to cancer patients.* Br J Clin Pharmacol, 2006. **62**(1): p. 71-80.
60. Breedveld, P., et al., *The effect of low pH on breast cancer resistance protein (ABCG2)-mediated transport of methotrexate, 7-hydroxymethotrexate, methotrexate diglutamate, folic acid, mitoxantrone, topotecan, and resveratrol in in vitro drug transport models.* Mol Pharmacol, 2007. **71**(1): p. 240-9.
61. Sane, R., et al., *The effect of ABCG2 and ABCC4 on the pharmacokinetics of methotrexate in the brain.* Drug Metab Dispos, 2014. **42**(4): p. 537-40.
62. *Methotrexate Compound Summary. Simcyp, Sheffield, UK. 2018.*
63. Zamek-Gliszczynski, M.J., et al., *Transporters in Drug Development: International Transporter Consortium Update on Emerging Transporters of Clinical Importance.* Clin Pharmacol Ther, 2022. **112**(3): p. 485-500.
64. Bowman, C.M., et al., *Examination of Physiologically-Based Pharmacokinetic Models of Rosuvastatin.* CPT Pharmacometrics Syst Pharmacol, 2021. **10**(1): p. 5-17.
65. Nuernberg, B., et al., *Biliary elimination of low-dose*

methotrexate in humans. Arthritis Rheum, 1990. **33**(6): p. 898-902.
66. Breithaupt, H. and E. Küenzlen, *Pharmacokinetics of methotrexate and 7-hydroxymethotrexate following infusions of high-dose methotrexate.* Cancer Treat Rep., 1982. **66**(9): p. 1733-41.
67. Michael S Roberts, et al., *Enterohepatic circulation: physiological, pharmacokinetic and clinical implications.* Clin Pharmacokinet, 2002. **41**(10): p. 751-90.
68. *METHOTREXATE tablets (methotrexate) [package insert]. London, UK: HIKMA Pharmaceuticals; 2020.*
69. Tessa M Bosch, et al., *Genetic polymorphisms of drug-metabolising enzymes and drug transporters in the chemotherapeutic treatment of cancer.* Clin Pharmacokinet, 2006. **45**(3): p. 253-85.
70. Nakanishi, T., *Drug transporters as targets for cancer chemotherapy.* Cancer Genomics Proteomics, 2007. **4**(3): p. 241-54.
71. Shu-Guang Liu, et al., *Polymorphisms in methotrexate transporters and their relationship to plasma methotrexate levels, toxicity of high-dose methotrexate, and outcome of pediatric acut lymphoblastic leukemia.* Oncotarget., 2017. **8**(23): p. 37761-72.
72. Anabtawi, N., et al., *The role of OATP1B1 and OATP1B3 transporter polymorphisms in drug disposition and response to anticancer drugs: a review of the recent literature.* Expert Opin Drug Metab Toxicol, 2022. **18**(7-8): p. 459-468.
73. Martinez, D., et al., *Endogenous Metabolites-Mediated Communication Between OAT1/OAT3 and OATP1B1 May Explain the Association Between SLCO1B1 SNPs and Methotrexate Toxicity.* Clin Pharmacol Ther, 2018. **104**(4): p. 687-698.
74. van de Meeberg, M.M., et al., *A meta-analysis of methotrexate polyglutamates in relation to efficacy and toxicity of methotrexate in inflammatory arthritis, colitis and dermatitis.* Br J Clin Pharmacol, 2022.
75. Alenka J Brooks, et al., *Red blood cell methotrexate polyglutamate concentrations in inflammatory bowel disease.* Ther Drug Monit, 2007. **29**(5): p. 619-25.
76. Dalrymple, J.M., et al., *Pharmacokinetics of oral methotrexate in patients with rheumatoid arthritis.* Arthritis

Rheum, 2008. **58**(11): p. 3299-308.
77. *US Food and Drug Administration. (2020). Clinical Drug Interaction Studies - Cytochrome P450 Enzyme- and Transporter- Mediated Drug Interactions. Accessed: July 15 2021. https://www.fda.gov/media/134581/download.*

Abstract in Korean

서론: 메토트렉세이트는 류마티스 관절염 및 암과 같은 다양한 질병의 치료에 널리 사용되는 항엽산제이다. 다양한 수송체의 기질로 알려진 메토트렉세이트는 다른 약물과 병용 투여 시 주의 깊게 모니터링해야 한다. 본 연구는 생리학적 기반 약동학(PBPK) 모델링을 사용하여 약물 수송체에 의해 매개되는 메토트렉세이트 약물-약물 상호작용을 정량적으로 해석하고자 하였다. 또한 본 연구를 통해 메토트렉세이트의 약물수송체 매개 약물-약물 상호작용에 대한 기전 평가 및 예측 시스템을 개발하여 메토트렉세이트의 개인 맞춤형 약물 요법에 적용하고자 하였다.

방법: 건강한 지원자에서 메토트렉세이트 약동학에 대한 리팜피신 및 페북소스타트의 영향를 평가하기 위해 무작위배정, 공개, 4-치료군, 6-순서군, 4-기간 교차 시험을 수행하였다. 대상자들은 할당된 순서에 따라 각 치료를 받았고, 4-치료군은 메토트렉세이트 2.5mg 단독 투여, 메토트렉세이트와 리팜피신 600mg 병용투여, 메토트렉세이트와 페북소스타트 80mg 병용투여 또는 3제 병용투여로 구성되었다. 약동학 분석을 위한 혈액 샘플을 임상시험용의약품 투여 후 24시간까지 수집하였다. 메토트렉세이트, 리팜피신 및 페북소스타트의 PBPK 모델은 생체 외(*in vitro*) 및 생체 내(*in vivo*) 연구를 기반으로 개발하였으며, 최종 PBPK 모델의 예측 성능은 임상 연구를 통해 검증하였다. 최종 PBPK 모델은 메토트렉세이트의 약물수송체 매개 약물-약물 상호작용

을 정량적으로 해석하고 암 환자에서 페북소스타트와 고용량 메토트렉세이트를 병용투여 시 약물-약물상호작용을 시뮬레이션 하였다.

결과: 본 연구에서 수행한 임상시험에서 메토트렉세이트와 리팜피신 또는 페북소스타트와 병용 투여했을 때 메토트렉세이트의 전신 노출은 단독 투여에 비해 각각 33% 및 17% 증가하였다. 메토트렉세이트를 리팜피신, 페북소스타트와 병용 투여했을 때 전신 노출은 단독 투여에 비해 52% 증가하였다. 최종 PBPK 모델은 관찰된 임상 데이터를 잘 예측하는 것을 확인하였다. 최종 PBPK 모델에서 민감도 분석을 이용하여 메토트렉세이트 약물-약물 상호작용에서 메토트렉세이트 약동학에 대한 약물수송체의 기여를 정량적으로 해석할 수 있었다. 또한 최종 PBPK 모델을 이용하여 가상 암 환자에서 메토트렉세이트 고용량과 페북소스타트를 병용투여 시 약동학을 시뮬레이션 하였을 때 메토트렉세이트 전신 노출이 약 30% 증가하였다.

결론: 본 연구는 페북소스타트의 유방암내성단백질(BCRP) 억제제로서의 잠재적인 활성을 평가하였다. 또한, 본 연구에서 메토트렉세이트의 PBPK 모델이 적절하게 개발되었고 다른 약물과 메토트렉세이트의 약물수송체 매개 약물-약물 상호작용을 예측 및 평가하는 모델으로서 맞춤약물요법에 활용할 수 있을 것으로 예상한다.

주요어: 약물-약물 상호작용, 약물수송체, 생리학 기반 약동학(PBPK)

모델링, 메토트렉세이트, 약동학, 맞춤약물요법

학 번: 2019-28140